

Modeling flexoelectricity in soft dielectrics at finite deformation

D. Codony¹, P. Gupta¹, O. Marco¹, I. Arias^{1,2,*}

¹ Laboratori de Càlcul Numèric (LaCàN), Universitat Politècnica de Catalunya (UPC),
Campus Nord UPC-C2, E-08034 Barcelona, Spain

² Centre Internacional de Mètodes Numèrics en Enginyeria (CIMNE),
08034 Barcelona, Spain

* Corresponding author; E-mail: irene.arias@upc.edu.

Abstract

This paper develops the equilibrium equations describing the flexoelectric effect in soft dielectrics under large deformations. Previous works have developed related theories using a flexoelectric coupling tensor of mixed material-spatial character. Here, we formulate the model in terms of a flexoelectric tensor completely defined in the material frame, with the same symmetries of the small-strain flexocoupling tensor and leading naturally to objective flexoelectric polarization fields. The energy potential and equilibrium equations are first expressed in terms of deformation and polarization, and then rewritten in terms of deformation and electric potential, yielding an unconstrained system of fourth order partial differential equations (PDE). We further develop a theory of geometrically nonlinear extensible flexoelectric rods under open and closed circuit conditions, with which we examine cantilever bending and buckling under mechanical and electrical actuation. Besides being a simple and explicit model pertinent to slender structures, this rod theory also allows us to test our general theory and its numerical implementation using B-Splines. This numerical implementation is robust as it handles the electromechanical instabilities in soft flexoelectric materials.

Keywords: Soft dielectrics , Maxwell equations , Flexoelectricity , Electrostriction , Buckling , Special Cosserat Rod

1 Introduction

Flexoelectricity is a two-way coupling between electric polarization and strain gradient, present in any dielectric material. The direct flexoelectric effect is understood as the material polarization due to inhomogeneous deformation (e.g. bending, twisting), and the converse flexoelectric effect

consists on the generation of stress due to the presence of an inhomogeneous electric field. The flexoelectric effect is size dependent due to its intrinsic scaling with strain-gradients, and therefore it is only relevant at the micro- and nanoscale.

Flexoelectric effects have been observed and widely studied in hard materials (Tolpygo, 1963, Kogan, 1964, Hong and Vanderbilt, 2011, Resta, 2010, Maranganti et al., 2006), mainly crystalline ceramics such as ferroelectric perovskites (Zubko et al., 2007, Ma and Cross, 2001a, 2002, Fu et al., 2006, Ma and Cross, 2001b, 2003, 2005, 2006). However, they are also present in soft materials, such as liquid crystals (Meyer, 1969, Petrov, 1975, Prost and Marcerou, 1977, Harden et al., 2006, Trabi et al., 2008), cellular membranes (Petrov et al., 1989, Todorov et al., 1991, 1994, Sun, 1997, Petrov, 2002) and polymers (Breger et al., 1976, Marvan and Havránek, 1998, Baskaran et al., 2011, 2012, Deng et al., 2014c, Zhang et al., 2016b, Zhou et al., 2017).

The mechanism of flexoelectricity in hard materials can be intuitively understood by the ionic crystal model under bending, in which a non-zero net dipole moment arises due to a shift between the centers of gravity of the negative and the positive ions. However, the flexoelectricity mechanism in soft materials is quite different. In soft materials such as liquid crystals or cellular membranes, flexoelectricity results from the reorientation of irregularly shaped polarized molecules under strain gradients (Nguyen et al., 2013). In polymers, flexoelectricity is more complicated than in crystalline solid materials or liquid crystals since both glassy and crystalline components contribute to flexoelectricity (Baskaran et al., 2011, 2012). We refer to (Yudin and Tagantsev, 2013, Nguyen et al., 2013, Zubko et al., 2013, Krichen and Sharma, 2016, Wang et al., 2019) for excellent and comprehensive reviews of flexoelectricity in solids.

In recent years, several reasons justify an increasing interest in flexoelectricity in polymer materials. On the one hand, a large flexoelectric response is expected. Experiments suggest that the flexoelectric coefficients of polymers are at least the same order of magnitude as those of hard crystalline materials (Chu and Salem, 2012, Baskaran et al., 2011, 2012), but being much more deformable, much larger flexoelectric polarization is possible. On the other hand, electromechanical actuation of polymers by flexoelectricity overcomes the current limitations of traditional actuation based on electrostriction, which are: (i) one-way coupling, i.e. mechanical deformation does not produce an electric field, (ii) very large electric fields are required (which may lead to dielectric breakdown), and (iii) reversal of electric field does not reverse the direction of the deformation (Pelrine et al., 1998, O'Halloran et al., 2008, Krichen and Sharma, 2016, Rosset and Shea, 2016). Furthermore, only a few polymers exhibit significant piezoelectricity (Bauer and Bauer, 2008). Thus, quantifying flexoelectricity at large deformations may enable the design of efficient electromechanical elastomeric devices, such as sensors, actuators and energy harvesters, based on the flexoelectric effect (Jiang et al., 2013, Huang et al., 2018, Wang et al., 2019).

The literature about continuum theories of flexoelectricity in bulk solids ranges from the early works by Mashkevich and Tolpygo (1957), Tolpygo (1963), Kogan (1964), Indenbom et al. (1981a,b), Tagantsev (1985, 1986), Sahin and Dost (1988), Tagantsev (1991) to the more recent developments by Maranganti et al. (2006), Shen and Hu (2010), Hu and Shen (2010), Hadjesfandiari (2013), Liu (2014), Anqing et al. (2015), to name a few. However, most of these works assume infinitesimal deformations, and are therefore suitable to model crystalline ceramics only. Efforts have been re-

cently made to extend the theory to polymers or elastomers undergoing large deformations, but the literature is still scarce (Liu, 2014, Yvonnet and Liu, 2017, Thai et al., 2018, Poya et al., 2019, McBride et al., 2019, Zhuang et al., 2019, Nguyen et al., 2019). Some of these works model flexoelectricity as a linear coupling between strain gradients and the electric displacement (Poya et al., 2019) or the electric field (McBride et al., 2019, Nguyen et al., 2019, Zhuang et al., 2019) instead of the electric polarization, which however is the most natural choice according to experiments and first-principle calculations (Ma and Cross, 2001a, 2002, Zubko et al., 2007, Resta, 2010, Hong and Vanderbilt, 2011). Furthermore, works modeling flexoelectricity as a coupling between strain gradients and electric polarization consider a coupling tensor of mixed material-spatial character (Liu, 2014, Yvonnet and Liu, 2017, Thai et al., 2018), leading in general to a lack of objectivity in the resulting polarization as argued in Section 2.3.

The equations of flexoelectricity can only be solved analytically in very simple settings, such as simplified Euler-Bernoulli (E-B) (Liang et al., 2014, Deng et al., 2014a) and Timoshenko beam (Zhang et al., 2016a) models. Such models have been extended to large deformations but moderate rotations *à la* von Karmann Baroudi and Najjar (2019). Otherwise, it is necessary to resort to computational flexoelectricity (Zhuang et al., 2020). The major challenge is to handle the C^1 continuity of the state variables required by the fourth-order PDE system. To address this, several numerical alternatives have been proposed, such as mesh-free approximations (Abdollahi et al., 2014, 2015a,b, Abdollahi and Arias, 2015, Zhuang et al., 2019), isogeometric analysis (Ghasemi et al., 2017, Nanthakumar et al., 2017, Thai et al., 2018, Hamdia et al., 2018, Ghasemi et al., 2018, Nguyen et al., 2019), C^1 Argyris triangular element approximation (Yvonnet and Liu, 2017) and the B-spline-based immersed boundary method (Codony et al., 2019). Another family of numerical methods are those circumventing the C^1 continuity requirement by introducing additional variables, such as mixed formulations (Mao et al., 2016, Deng et al., 2017, 2018), or those based on micromorphic theories of continua (Poya et al., 2019, McBride et al., 2019). Recently, a few works report the application of these methods to large deformation flexoelectricity (Thai et al., 2018, Poya et al., 2019, McBride et al., 2019, Yvonnet and Liu, 2017, Zhuang et al., 2019, Nguyen et al., 2019) but the continuum formulation at finite deformation is still open, see previous paragraph, and there is a need for validation of the computational results.

To provide a general tool to assess flexoelectricity under large deformations, we propose a formulation with a fully material flexoelectric coupling between strain gradient and electric polarization, leading by construction to objective polarization fields. To facilitate the solution of the associated boundary value problem, we reformulate the balance equations in terms of displacements and electric potential as primal unknowns, yielding an unconstrained system of fourth-order PDE. We solve this system computationally with open uniform B-spline basis in body-fitted Cartesian meshes. We further derive large deformation models for geometrically nonlinear extensible flexoelectric rods under open and closed circuit conditions and derive closed-form solutions for cantilever bending and buckling. We report excellent agreement well into the nonlinear regime between numerical and analytical solutions in conditions mimicking the assumptions of the analytical models, which serves as validation. We then explore general flexoelectric problems beyond the simplifying assumptions of the analytical models and analyze the role of the flexoelectric ma-

terial parameters in the electromechanical response of the rod.

The paper is organized as follows. In Section 2 the free energy density and corresponding balance equations of a flexoelectric body are reviewed, the mathematical expression of the flexoelectric coupling is discussed, and the boundary value problem is stated. The numerical implementation used to solve the boundary value problem is presented in Section 3, and the analytical solutions for one-dimensional geometrically nonlinear flexoelectric rods are derived in Section 4. In Section 5 the numerical and analytical results of bending and buckling of rods under open/closed circuit are shown. The paper is concluded in Section 6.

2 Variational formulation of flexoelectricity in material form

2.1 Background and balance laws in spatial and material forms

Consider a deformable dielectric body described by Ω_0 in the reference (or undeformed) configuration, and by Ω in the current (or deformed) configuration. The deformation map $\chi : \Omega_0 \rightarrow \Omega$ maps every material point $\mathbf{X} \in \Omega_0$ to the spatial point $\mathbf{x} = \chi(\mathbf{X}) \in \Omega$. Whenever index notations are used, uppercase and lowercase indexes refer to quantities in the reference and the current configurations, respectively. The deformation gradient \mathbf{F} , the Jacobian determinant J , and the right and left Cauchy-Green deformation tensors \mathbf{C} , \mathbf{B} are defined as

$$F_{iI}(\mathbf{X}) := \frac{\partial \chi_i(\mathbf{X})}{\partial X_I}, \quad J := \det(\mathbf{F}), \quad C_{IJ} := F_{kI}F_{kJ}, \quad B_{ij} := F_{iK}F_{jK}. \quad (1)$$

Standard strain measures in the reference and the current configurations are the Green-Lagrangian \mathfrak{E} and the Almansi-Eulerian \mathfrak{e} strain tensors given by

$$\mathfrak{E}_{IJ} := \frac{1}{2} (C_{IJ} - \delta_{IJ}), \quad \mathfrak{e}_{ij} := \frac{1}{2} (\delta_{ij} - B_{ij}^{-1}) = \mathfrak{E}_{IJ} F_{iI}^{-1} F_{jJ}^{-1}. \quad (2)$$

Since the flexoelectricity theory involves high-order derivatives, let us define the gradient of the deformation gradient $\widetilde{\mathbf{F}}$, the gradient of the Cauchy-Green deformation tensor $\widetilde{\mathbf{C}}$ and the Green-Lagrangian strain gradient $\widetilde{\mathfrak{E}}$ as

$$\widetilde{F}_{iJK} := \frac{\partial F_{iJ}}{\partial X_K} = \frac{\partial^2 \chi_i}{\partial X_J \partial X_K}, \quad \widetilde{C}_{IJK} := \frac{\partial C_{IJ}}{\partial X_K} = 2 \operatorname{symm}_{IJ}(\widetilde{F}_{kIK} F_{kJ}), \quad \widetilde{\mathfrak{E}}_{IJK} := \frac{\partial \mathfrak{E}_{IJ}}{\partial X_K} = \frac{1}{2} \widetilde{C}_{IJK}; \quad (3)$$

where $\operatorname{symm}_{IJ}(A_{IJ}) := (A_{IJ} + A_{JI})/2$. Note that the relation $\widetilde{\mathfrak{E}}(\widetilde{\mathbf{F}})$ in Eq. (3) is inverted as

$$\widetilde{F}_{iJK} = (\widetilde{\mathfrak{E}}_{IJK} + \widetilde{\mathfrak{E}}_{KIJ} - \widetilde{\mathfrak{E}}_{KJI}) F_{iI}^{-1}, \quad (4)$$

analogously to the relation between second derivative of displacement and strain gradients in the limit of infinitesimal deformation (Schiaffino et al., 2019).

This body in equilibrium necessarily satisfies mechanical balance laws of linear and angular momentum, and Maxwell equations. In the absence of a magnetic field, they can be expressed in an Eulerian frame as

$$\nabla \cdot \boldsymbol{\sigma} + \mathbf{b} = \mathbf{0}, \quad (5a)$$

$$\boldsymbol{\sigma} = \boldsymbol{\sigma}^T, \quad (5b)$$

$$\nabla \times \mathbf{e} = \mathbf{0}, \quad (5c)$$

$$\nabla \cdot \mathbf{d} - q = 0; \quad (5d)$$

where $\boldsymbol{\sigma}$ is the physical stress, \mathbf{e} is the electric field, \mathbf{d} is the electric displacement, and \mathbf{b} and q are the body force and electric charge per unit volume. Equation (5c) implies the existence of an electric potential ϕ such that $\mathbf{e} = -\nabla\phi$. The linear constitutive law for \mathbf{d} for a dielectric material is

$$\mathbf{d}(\mathbf{p}, \mathbf{e}) = \epsilon_0 \mathbf{e} + \mathbf{p} \quad \text{or, equivalently,} \quad \mathbf{d}(\mathbf{p}, \phi) = -\epsilon_0 \nabla\phi + \mathbf{p}, \quad (6)$$

where \mathbf{p} is the electric polarization, which is work-conjugate to \mathbf{e} , and ϵ_0 is the electric permittivity of vacuum.

To formulate the problem in a material frame, the Lagrangian second Piola-Kirchhoff physical stress tensor \mathbf{S} is defined from the work-conjugacy relation

$$\sigma_{ij} \mathbf{e}_{ij} = \frac{1}{J} S_{IJ} \mathfrak{E}_{IJ}, \quad (7)$$

where $\sigma_{ij} \mathbf{e}_{ij}$ is a mechanical work density per unit physical volume and $S_{IJ} \mathfrak{E}_{IJ}$ a mechanical work density per unit reference volume, leading to

$$S_{IJ} = J F_{Ii}^{-1} F_{Jj}^{-1} \sigma_{ij}, \quad (8)$$

where strictly speaking we should write $S_{IJ} \circ \chi^{-1} = J F_{Ii}^{-1} F_{Jj}^{-1} \sigma_{ij}$ to account for the fact that some of these fields are over Ω_0 and others are over Ω . To follow an analogous procedure with the electric displacement (Lax and Nelson, 1976, Dorfmann and Ogden, 2005, Vu et al., 2007, Dorfmann and Ogden, 2014, 2017, Steinmann and Vu, 2017), we first identify the nominal or material electric field. The electric potential can be expressed in the material frame as $\Phi(\mathbf{X}) = \phi(\chi(\mathbf{X}))$, and the nominal electric field \mathbf{E} defined as the negative of its material gradient. By the chain rule, we thus find that

$$E_I = -\frac{\partial \Phi}{\partial X_I} = -\frac{\partial \phi}{\partial x_i} \frac{\partial x_i}{\partial X_I} = e_i F_{iI}. \quad (9)$$

Then, from the work-conjugacy relation

$$d_i e_i = \frac{1}{J} D_I E_I, \quad (10)$$

we identify the nominal electric displacement as

$$D_I = J F_{Ii}^{-1} d_i. \quad (11)$$

Since electric displacement and polarization are physically equivalent quantities, we analogously find

$$P_I = J F_{Ii}^{-1} p_i. \quad (12)$$

Using Eq. (1), (8), (9), (11), (12), the balance equations in Eq. (5a)-(5d) and the constitutive law for dielectrics in Eq. (6) are written in material form as

$$(F_{iI} S_{IJ})_{,J} + B_i = 0_i, \quad (13a)$$

$$S_{IJ} = S_{JI}, \quad (13b)$$

$$E_L + \Phi_{,L} = 0, \quad (13c)$$

$$D_K = \epsilon_0 J C_{KL}^{-1} E_L + P_K, \quad (13d)$$

$$D_{K,K} - Q = 0, \quad (13e)$$

with $B = Jb$ and $Q = Jq$.

2.2 Constitutive relations and thermodynamic potentials in material form

We define the Lagrangian internal energy density per unit reference volume of the flexoelectric solid as

$$\Psi^{\text{Int}}(\mathfrak{F}, \widetilde{\mathfrak{F}}, \mathbf{P}) = \Psi^{\text{Mech}}(\mathfrak{F}, \widetilde{\mathfrak{F}}) + \Psi^{\text{Diele}}(\mathfrak{F}, \mathbf{P}) + \Psi^{\text{Flexo}}(\mathbf{P}, \widetilde{\mathfrak{F}}). \quad (14)$$

We allow Ψ^{Mech} to depend on Lagrangian strain and strain gradient as required for stability (Liu, 2014). The isotropic dielectric energy per unit reference volume follows by transforming the spatial expression per unit physical volume $\psi^{\text{Diele}}(\mathbf{p}) = \frac{1}{2(\epsilon - \epsilon_0)} p_i p_i$ (Liu, 2014) by recalling Eq. (12), resulting in

$$\Psi^{\text{Diele}}(\mathfrak{F}, \mathbf{P}) = \frac{1}{2J(\epsilon - \epsilon_0)} P_I C_{IJ} P_J, \quad (15)$$

where ϵ denotes the electric permittivity of the material. The flexoelectric coupling linking polarization and strain gradient is encoded by Ψ^{Flexo} , which for simplicity we assume to be independent on strain.

The spatial expression of the electrostatic energy density $\psi^{\text{Elec}}(\mathbf{e}) = \frac{1}{2} \epsilon_0 e_i e_i$ (Liu, 2014) can also be expressed in the material frame by recalling Eq. (9), resulting in the energy density per unit reference volume

$$\Psi^{\text{Elec}}(\mathfrak{F}, \mathbf{E}) = \frac{J \epsilon_0}{2} E_I C_{IJ}^{-1} E_J. \quad (16)$$

To formulate a unified potential self-consistently accounting for the material electromechanics and for electrostatics, $\Psi^{\text{Int}}(\mathfrak{E}, \widetilde{\mathfrak{E}}, \mathbf{P})$ and $\Psi^{\text{Elec}}(\mathfrak{E}, \mathbf{E})$ must be expressed in terms of the same variables. To accomplish this, we resort to a partial Legendre transform and define the following internal dual potential

$$\bar{\Psi}^{\text{Int}}(\mathfrak{E}, \widetilde{\mathfrak{E}}, \mathbf{E}) = \min_{\mathbf{P}} \left(\Psi^{\text{Int}}(\mathfrak{E}, \widetilde{\mathfrak{E}}, \mathbf{P}) - \mathbf{P} \cdot \mathbf{E} \right). \quad (17)$$

The stationarity condition of the minimization results in

$$\mathbf{E}(\mathfrak{E}, \widetilde{\mathfrak{E}}, \mathbf{P}) = \frac{\partial \Psi^{\text{Int}}}{\partial \mathbf{P}}. \quad (18)$$

In principle, this expression can be inverted to find $\mathbf{P}(\mathbf{E}, \mathfrak{E}, \widetilde{\mathfrak{E}})$, which plugged into $\Psi^{\text{Int}}(\mathfrak{E}, \widetilde{\mathfrak{E}}, \mathbf{P}) - \mathbf{P} \cdot \mathbf{E}$ results in the dual potential $\bar{\Psi}^{\text{Int}}(\mathfrak{E}, \widetilde{\mathfrak{E}}, \mathbf{E})$.

If we postulate the following flexoelectric coupling

$$\Psi^{\text{Flexo}}(\mathbf{P}, \widetilde{\mathfrak{E}}) = -P_L f_{LIJK} \widetilde{\mathfrak{E}}_{IJK}, \quad (19)$$

where f_{LIJK} is a purely Lagrangian tensor as further discussed later, this inversion can be made explicit yielding

$$E_L = \frac{1}{J(\epsilon - \epsilon_0)} C_{LM} P_M - f_{LIJK} \widetilde{\mathfrak{E}}_{IJK} \Rightarrow \\ P_M = J(\epsilon - \epsilon_0) C_{ML}^{-1} \left(E_L + f_{LIJK} \widetilde{\mathfrak{E}}_{IJK} \right) = J(\epsilon - \epsilon_0) C_{ML}^{-1} \left(E_L + E_L^{\text{Flexo}} \right), \quad (20)$$

where we have defined $E_L^{\text{Flexo}} = f_{LIJK} \widetilde{\mathfrak{E}}_{IJK}$ for convenience. Replacing this expression for \mathbf{P} in Eq. (17) and rearranging terms, we find

$$\bar{\Psi}^{\text{Int}}(\mathfrak{E}, \widetilde{\mathfrak{E}}, \mathbf{E}) = \Psi^{\text{Mech}}(\mathfrak{E}, \widetilde{\mathfrak{E}}) - \frac{J}{2} (\epsilon - \epsilon_0) E_I^{\text{Flexo}} C_{IJ}^{-1} E_J^{\text{Flexo}} - \frac{J}{2} (\epsilon - \epsilon_0) E_I C_{IJ}^{-1} E_J - J(\epsilon - \epsilon_0) E_I C_{IJ}^{-1} E_J^{\text{Flexo}}. \quad (21)$$

Now, the total electromechanical enthalpy accounting for electrostatics $\bar{\Psi}^{\text{Enth}} = \bar{\Psi}^{\text{Int}} - \Psi^{\text{Elec}}$ (Liu, 2014, Dorfmann and Ogden, 2014, 2017) can be written as

$$\bar{\Psi}^{\text{Enth}}(\mathfrak{E}, \widetilde{\mathfrak{E}}, \mathbf{E}) = \bar{\Psi}^{\text{Mech}}(\mathfrak{E}, \widetilde{\mathfrak{E}}) + \bar{\Psi}^{\text{Diele}}(\mathfrak{E}, \mathbf{E}) + \bar{\Psi}^{\text{Flexo}}(\mathfrak{E}, \widetilde{\mathfrak{E}}, \mathbf{E}), \quad (22)$$

with

$$\bar{\Psi}^{\text{Diele}}(\mathfrak{E}, \mathbf{E}) = -\frac{1}{2} J \epsilon E_M C_{ML}^{-1} E_L, \quad (23)$$

$$\bar{\Psi}^{\text{Flexo}}(\mathfrak{E}, \widetilde{\mathfrak{E}}, \mathbf{E}) = -J C_{ML}^{-1} E_M \mu_{LIJK} \widetilde{\mathfrak{E}}_{IJK}; \quad (24)$$

where $\boldsymbol{\mu} = (\epsilon - \epsilon_0)\mathbf{f}$ is the flexoelectricity tensor (Zubko et al., 2013, Wang et al., 2019), described in Eq. (A.3). The *effective* mechanical energy density of the system (Wang et al., 2019) is

$$\begin{aligned}\bar{\Psi}^{\text{Mech}}(\mathfrak{E}, \tilde{\mathfrak{E}}) &= \Psi^{\text{Mech}}(\mathfrak{E}, \tilde{\mathfrak{E}}) - \frac{J}{2}(\epsilon - \epsilon_0)E_M^{\text{Flexo}}C_{ML}^{-1}E_L^{\text{Flexo}}, \\ &= \Psi^{\text{Mech}}(\mathfrak{E}, \tilde{\mathfrak{E}}) - \frac{1}{2}\tilde{\mathfrak{E}}_{IJK}\left(\frac{\mu_{AIJK}JC_{AB}^{-1}\mu_{BLMN}}{\epsilon - \epsilon_0}\right)\tilde{\mathfrak{E}}_{LMN}.\end{aligned}\quad (25)$$

The standard mechanical contribution accounting for strain gradient elasticity can be written as

$$\Psi^{\text{Mech}}(\mathfrak{E}, \tilde{\mathfrak{E}}) = \Psi^{\text{Elast}}(\mathfrak{E}) + \frac{1}{2}\tilde{\mathfrak{E}}_{IJK}h_{IJKLMN}\tilde{\mathfrak{E}}_{LMN}, \quad (26)$$

where Ψ^{Elast} can be any classical hyperelastic potential, e.g. Saint-VenantKirchhoff, cf. Eq. (A.1), or Neo-Hookean, cf. Eq. (A.2), constitutive models, and \mathbf{h} is the sixth-order strain gradient elasticity tensor. Upon inspection, it is clear that the second contribution in Eq. (25), i.e. the flexoelectricity-induced mechanical energy, has the same structure as the strain gradient elasticity potential. For convenience, we thus define

$$\bar{\Psi}^{\text{Mech}}(\mathfrak{E}, \tilde{\mathfrak{E}}) = \Psi^{\text{Elast}}(\mathfrak{E}) + \frac{1}{2}\tilde{\mathfrak{E}}_{IJK}\bar{h}_{IJKLMN}\tilde{\mathfrak{E}}_{LMN}, \quad (27)$$

where

$$\bar{h}_{IJKLMN} = h_{IJKLMN} - \frac{\mu_{AIJK}JC_{AB}^{-1}\mu_{BLMN}}{\epsilon - \epsilon_0} \quad (28)$$

is the *effective* strain gradient elasticity tensor as described in Eq. (A.4). To preserve the positive definiteness of $\bar{\Psi}^{\text{Mech}}$, it is clear from Eq. (27) that $\bar{\mathbf{h}}$ has to be semidefinite positive and thus a stability condition can be derived from Eq. (28) depending on both \mathbf{h} and $\boldsymbol{\mu}$ (Yudin et al., 2014, 2015, Morozovska et al., 2016).

2.3 Variational formulation in material form

The boundary of the reference body, $\partial\Omega_0$, is split in several disjoint Dirichlet and Neumann sets as follows:

$$\partial\Omega_0 = \partial\Omega_0^{\chi} \cup \partial\Omega_0^T = \partial\Omega_0^V \cup \partial\Omega_0^R = \partial\Omega_0^{\Phi} \cup \partial\Omega_0^W. \quad (29)$$

On the Dirichlet boundaries $\partial\Omega_0^{\chi}$, $\partial\Omega_0^V$ and $\partial\Omega_0^{\Phi}$, the deformation map $\boldsymbol{\chi}$, normal derivatives of the deformation map $\partial_0^N\boldsymbol{\chi}$, and electric potential Φ are prescribed, respectively. On the Neumann boundaries $\partial\Omega_0^T$, $\partial\Omega_0^R$ and $\partial\Omega_0^W$, their respective work conjugate quantities (per unit reference volume) are prescribed, i.e. the surface traction $\mathbf{T}(\boldsymbol{\chi}, \Phi) = \bar{\mathbf{T}}$, the surface double traction $\mathbf{R}(\boldsymbol{\chi}, \Phi) = \bar{\mathbf{R}}$ and the surface charge $W(\boldsymbol{\chi}, \Phi) = \bar{W}$. As a result of the strain-gradient elasticity potential (Mindlin, 1964, Mindlin and Eshel, 1968), additional loads arise in non-smooth regions of $\partial\Omega_0$, i.e. edges C_0

in a three-dimensional domain (Mao and Purohit, 2014, Codony et al., 2019). We also split them in Dirichlet in Neumann sets as

$$C_0 = C_0^\chi \cup C_0^J, \quad (30)$$

depending on whether the deformation map χ or edge forces (per unit reference volume) $J(\chi, \Phi) = \bar{J}$ are prescribed. For simplicity, dead loads are considered.

The enthalpy functional governing the physics of a flexoelectric body is written as

$$\begin{aligned} \Pi[\chi, \Phi] = & \int_{\Omega_0} \left(\bar{\Psi}^{\text{Enth}}(\mathfrak{E}, \tilde{\mathfrak{E}}, -\nabla_0 \Phi) - B_i \chi_i + Q\Phi \right) d\Omega_0 \\ & - \int_{\partial\Omega_0^T} \bar{T}_i \chi_i d\Gamma_0 - \int_{\partial\Omega_0^R} \bar{R}_i \partial_0^N \chi_i d\Gamma_0 - \int_{C_0^J} \bar{J}_i \chi_i dS_0 + \int_{\partial\Omega_0^W} \bar{W} \Phi d\Gamma_0, \end{aligned} \quad (31)$$

where we have used $E = -\nabla_0 \Phi$ from Eq. (13c). Equilibrium states $\{\chi^*, \Phi^*\}$ are its saddle points satisfying

$$\{\chi^*, \Phi^*\} = \arg \min_{\chi \in \mathcal{X}} \max_{\Phi \in \mathcal{P}} \Pi[\chi, \Phi], \quad (32)$$

where \mathcal{X} and \mathcal{P} are the functional spaces for χ and Φ with sufficient regularity fulfilling Dirichlet boundary conditions.

A necessary condition for equilibrium is the vanishing of the first variation of $\Pi[\chi, \Phi]$

$$\begin{aligned} 0 = \delta \Pi[\chi, \Phi; \delta \chi, \delta \Phi] = & \int_{\Omega_0} \left(\frac{\partial \bar{\Psi}^{\text{Enth}}}{\partial \mathfrak{E}_{IJ}} \delta \mathfrak{E}_{IJ} + \frac{\partial \bar{\Psi}^{\text{Enth}}}{\partial \tilde{\mathfrak{E}}_{IJK}} \delta \tilde{\mathfrak{E}}_{IJK} + \frac{\partial \bar{\Psi}^{\text{Enth}}}{\partial E_L} \delta E_L - B_i \delta \chi_i + Q \delta \Phi \right) d\Omega_0 \\ & - \int_{\partial\Omega_0^T} \bar{T}_i \delta \chi_i d\Gamma_0 - \int_{\partial\Omega_0^R} \bar{R}_i \partial_0^N \delta \chi_i d\Gamma_0 - \int_{C_0^J} \bar{J}_i \delta \chi_i dS_0 + \int_{\partial\Omega_0^W} \bar{W} \delta \Phi d\Gamma_0 \\ = & \int_{\Omega_0} \left(\bar{S}_{IJ} \delta \mathfrak{E}_{IJ} + \bar{S}_{MJK} \delta \tilde{\mathfrak{E}}_{MJK} - D_L \delta E_L - B_i \delta \chi_i + Q \delta \Phi \right) d\Omega_0 \\ & - \int_{\partial\Omega_0^T} \bar{T}_i \delta \chi_i d\Gamma_0 - \int_{\partial\Omega_0^R} \bar{R}_i \partial_0^N \delta \chi_i d\Gamma_0 - \int_{C_0^J} \bar{J}_i \delta \chi_i dS_0 + \int_{\partial\Omega_0^W} \bar{W} \delta \Phi d\Gamma_0, \end{aligned} \quad (33)$$

for all admissible variations $\delta \chi$ and $\delta \Phi$, and where

$$\delta E_L := -\frac{\partial(\delta \Phi)}{\partial X_L}, \quad \delta F_{iI} := \frac{\partial(\delta \chi_i)}{\partial X_I}, \quad \delta \tilde{F}_{iIJ} := \frac{\partial^2(\delta \chi_i)}{\partial X_I \partial X_J}, \quad (34)$$

$$\delta \mathfrak{E}_{IJ} = \frac{1}{2} \delta C_{IJ} := \text{symm}_{IJ}(\delta F_{kI} F_{kJ}), \quad \delta \tilde{\mathfrak{E}}_{IJK} = \frac{1}{2} \delta \tilde{C}_{IJK} := \text{symm}_{IJ}(\delta F_{kI} \tilde{F}_{kJK} + F_{kI} \delta \tilde{F}_{kJK}). \quad (35)$$

We have introduced the local second Piola-Kirchhoff stress $\widehat{\mathbf{S}}$, the second Piola-Kirchhoff double stress $\widetilde{\mathbf{S}}$ and the electric displacement \mathbf{D} defined as follows:

$$\widehat{S}_{IJ}(\chi, \Phi) = \frac{\partial \bar{\Psi}^{\text{Enth}}}{\partial \mathfrak{E}_{IJ}} = 2 \frac{\partial \Psi^{\text{Elast}}(\mathbf{C})}{\partial C_{IJ}} + J \mathcal{C}_{MLIJ} E_M \left(\frac{1}{2} \epsilon E_L + \mu_{LABK} \widetilde{\mathfrak{E}}_{ABK} \right), \quad (36)$$

$$\widetilde{S}_{IJK}(\chi, \Phi) = \frac{\partial \bar{\Psi}^{\text{Enth}}}{\partial \widetilde{\mathfrak{E}}_{IJK}} = \bar{h}_{IJKLMN} \widetilde{\mathfrak{E}}_{LMN} - J C_{LM}^{-1} E_M \mu_{LIJK}, \quad (37)$$

$$D_L(\chi, \Phi) = - \frac{\partial \bar{\Psi}^{\text{Enth}}}{\partial E_L} = J C_{KL}^{-1} (\epsilon E_K + \mu_{KLIJ} \widetilde{\mathfrak{E}}_{IJM}), \quad (38)$$

with

$$\mathcal{C}_{ABCD} = \frac{2}{J} \frac{\partial (-J C_{AB}^{-1})}{\partial C_{CD}} = (C_{AC}^{-1} C_{BD}^{-1} + C_{BC}^{-1} C_{AD}^{-1} - C_{AB}^{-1} C_{CD}^{-1}). \quad (39)$$

Analogously to the infinitesimal strain theory of flexoelectricity (Mao and Purohit, 2014, Codony et al., 2019), Eq. (33) can be integrated by parts and, by invoking the divergence and surface divergence theorems, the strong form in Eq. (13) is recovered along with the following definitions of the physical second Piola-Kirchhoff stress \mathbf{S} , the surface traction \mathbf{T} , the double traction \mathbf{R} , the surface charge density W and the edge forces \mathbf{J} :

$$\begin{aligned} S_{IJ}(\chi, \Phi) &:= \widehat{S}_{IJ}(\chi, \Phi) - \widetilde{S}_{IJK,K}(\chi, \Phi) \\ &= 2 \frac{\partial \Psi^{\text{Elast}}(\mathbf{C})}{\partial C_{IJ}} - \bar{h}_{IJKLMN} \widetilde{\mathfrak{E}}_{LMN,K} + \frac{J}{2} \mathcal{C}_{MLIJ} E_M \epsilon E_L + J C_{LM}^{-1} E_M \mu_{LIJK} \quad \text{in } \Omega_0, \end{aligned} \quad (40a)$$

$$T_i(\chi, \Phi) := F_{iI} \left[(S_{IJ}(\chi, \Phi) - \widetilde{S}_{IKJ,N} \mathbb{P}_{NK}) N_J + \widetilde{S}_{IJK} \widetilde{N}_{JK} \right] - \widetilde{F}_{iIN} \mathbb{P}_{NK} \widetilde{S}_{IKJ} N_J \quad \text{on } \partial\Omega_0, \quad (40b)$$

$$R_i(\chi, \Phi) := F_{iI} \widetilde{S}_{IJK} N_J N_K \quad \text{on } \partial\Omega_0, \quad (40c)$$

$$W(\chi, \Phi) := - D_L N_L \quad \text{on } \partial\Omega_0, \quad (40d)$$

$$J_i(\chi, \Phi) := \llbracket F_{iI} \widetilde{S}_{IJK} M_J N_K \rrbracket \quad \text{on } C_0; \quad (40e)$$

where \mathbf{N} is the outward unit normal vector on $\partial\Omega_0$, \mathbf{M} is the outward unit co-normal vector on C_0 , $\mathbb{P} = \mathbf{I} - \mathbf{N} \times \mathbf{N}$ is the projection operator on $\partial\Omega_0$, $\widetilde{\mathbf{N}} = \nabla_0 \mathbf{N} : \mathbb{P}(\mathbf{N} \times \mathbf{N}) - \nabla_0 \mathbf{N} \cdot \mathbb{P}$ is the second-order geometry tensor on $\partial\Omega_0$ and $\llbracket \cdot \rrbracket$ is the jump operator defined on C as the sum of its argument evaluated at each boundary adjacent to C (we refer to Codony et al. (2019) for a detailed definition of the quantities involved here).

Upon inspection, the second Piola-Kirchhoff stress tensor \mathbf{S} in Eq. (40a) is composed by four terms. The first two terms correspond to the classical and high-order mechanical stresses, respectively. The third one corresponds to the total second Piola-Maxwell stress tensor $\mathbf{S}^{\text{Maxwell}}$. This becomes evident by expanding it as

$$S^{\text{Maxwell}}_{IJ} := \frac{J}{2} \mathcal{C}_{MLIJ} E_M \epsilon E_L = J F_{iI}^{-1} F_{jJ}^{-1} \epsilon \left[(E_M F_{Mi}^{-1}) (E_L F_{Lj}^{-1}) - \frac{1}{2} (E_M F_{Ma}^{-1}) (E_L F_{La}^{-1}) \delta_{ij} \right], \quad (41)$$

and obtaining its spatial counterpart by using Eq. (8) and (9) as

$$\boldsymbol{\sigma}^{\text{Maxwell}} := \epsilon \left(\mathbf{e} \otimes \mathbf{e} - \frac{1}{2} |\mathbf{e}|^2 \mathbf{I} \right). \quad (42)$$

The last term in Eq. (40a) corresponds to the total flexoelectricity-induced stress, and is analogous to the term appearing in the linear theory of flexoelectricity, cf. Eqs. (31-33) in (Codony et al., 2019).

Equations (20) and (38) show that the Lagrangian flexoelectric polarization in the present theory is $P_M = JC_{ML}^{-1}(\epsilon - \epsilon_0)E_L + JC_{ML}^{-1}\mu_{LIJK}\tilde{\mathfrak{E}}_{IJK}$, and hence its spatial counterpart is derived with Eq. (9) and (12) as

$$p_m = (\epsilon - \epsilon_0)e_m + F_{Lm}^{-1}\mu_{LIJK}\tilde{\mathfrak{E}}_{IJK}. \quad (43)$$

In the present formulation, μ_{LIJK} is a purely Lagrangian tensor, and hence it is meaningful to view it as a material constant with the same material symmetries and intrinsic symmetry ($\mu_{LIJK} = \mu_{LJKI}$) as the small strain flexoelectric tensor (Majdoub et al., 2008, Zubko et al., 2013, Krichen and Sharma, 2016). We note, however, that in previous literature a distinct notion of polarization per unit undeformed volume is introduced as $\mathbf{p}^r = J\mathbf{p}$, i.e. a volume-normalized spatial polarization related to our material or nominal polarization by $p_i^r = F_{iI}P_I$ (Liu, 2014, Dorfmann and Ogden, 2014, 2017). The polarization \mathbf{p}^r is not work-conjugate to the Lagrangian electric field \mathbf{E} . Furthermore, when it is used to formulate flexoelectric models it can be problematic. Indeed, the flexoelectric coupling has been defined in terms of \mathbf{p}^r (Liu, 2014, Deng et al., 2014b,c, Yvonnet and Liu, 2017, Thai et al., 2018) as

$$\Psi^{\text{Flexo}}(\tilde{\mathbf{F}}, \mathbf{p}^r) = -p_i^r \mathcal{F}_{iIJK} \tilde{F}_{IJK}, \quad (44)$$

with \mathcal{F} a mixed spatial-material flexoelectric tensor, which unlike the infinitesimal flexoelectric tensor is intrinsically symmetric with respect to its last two indices ($\mathcal{F}_{iIJK} = \mathcal{F}_{iIKJ}$). By comparing Eq. (44) and (19), using Eq. (3) and (4), the relation $p_i^r = F_{iI}P_I$ and the chain rule, we find the relation between \mathbf{f} and \mathcal{F} as

$$\mathcal{F}_{iIJK} = -\frac{\partial^2 \Psi^{\text{Flexo}}}{\partial p_i^r \partial \tilde{F}_{IJK}} = \text{symm}_{JK}(f_{LIJK}) F_{iI} F_{LI}^{-1}, \quad (45a)$$

$$f_{LIJK} = -\frac{\partial^2 \Psi^{\text{Flexo}}}{\partial P_L \partial \tilde{\mathfrak{E}}_{IJK}} = \left(\mathcal{F}_{iIJK} F_{Li}^{-1} + \mathcal{F}_{iIJK} F_{Lj}^{-1} - \mathcal{F}_{iKIJ} F_{Lk}^{-1} \right) F_{iL}. \quad (45b)$$

In the limit of infinitesimal deformation, \mathcal{F} and \mathbf{f} correspond to the so-called type-I (\mathbf{f}^I) and type-II (\mathbf{f}^{II}) flexocoupling tensors, respectively, and choosing one or the other is just a matter of convenience (Schiaffino et al., 2019). However this equivalence does not hold anymore in a finite deformation framework, since \mathbf{f} is purely Lagrangian whereas \mathcal{F} is not.

Equation (45b) clearly shows that taking \mathcal{F} as a material constant, as done in Yvonnet and Liu (2017) and Thai et al. (2018), directly implies a very particular dependence of the Lagrangian flexoelectric tensor \mathbf{f} on deformation. Thus, formulating flexoelectricity as in Eq. (44) leads implicitly to a material flexoelectric tensor whose magnitude and symmetry depend on deformation in a way

that is unphysical. To illustrate this assertion, consider a particular case in which χ corresponds to a rigid body deformation map, and thus \mathbf{F} is a rotation matrix $\mathbf{R} \neq \mathbf{I}$. Then, Eq. (45b) leads to

$$f_{LIJK} = (\mathcal{F}_{liJK}R_{li} + \mathcal{F}_{ljIK}R_{lj} - \mathcal{F}_{lkIJ}R_{lk})R_{lL} \quad (46)$$

showing that, if Eq. (44) is used to model flexoelectricity, then the Lagrangian flexoelectric material tensor, and hence the enthalpy functional $\Pi[\chi, \Phi]$, are not invariant with respect to a superimposed rigid body motion and hence not objective.

3 Numerical implementation

In this Section, we develop a direct numerical approach to solve the boundary value problem in Section 2.3. We restrict ourselves to 2D rod-like geometries, which can be easily discretized by Cartesian grids. The state variables $\{\chi, \Phi\}$ are approximated by an open uniform B-spline basis (de Boor, 2001, Rogers, 2001, Piegl and Tiller, 2012) of degree $p \geq 2$ in order to provide the smoothness required by the high-order model (see Fig. 1). Since the basis is interpolant at the boundaries of the reference domain, Dirichlet boundary conditions are strongly enforced. Domain and boundary integrals are approximated by standard Gaussian quadrature rules.

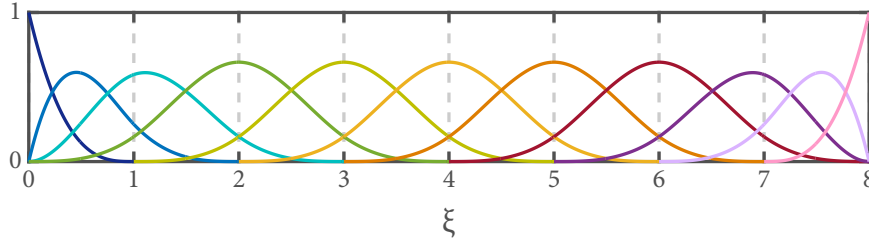


Figure 1: Univariate open uniform B-spline basis of degree $p = 3$. Each basis function is a smooth (C^{p-1}) piece-wise polynomial on a compact ($\leq p + 1$) support. Multivariate B-spline bases are constructed by means of the tensor product of multiple univariate bases.

The discretization of Eq. (33) yields a nonlinear system of equations (for the sake of brevity, we keep the same notation to denote discretized quantities). In order to solve it, we consider a modified-step Newton-Raphson algorithm. At the k -th iteration, an increment of the solution $\{\Delta\chi, \Delta\Phi\}^{(k)}$ is found by vanishing the first order Taylor expansion of the residual \mathcal{R} in Eq. (33) around the previous solution $\{\chi, \Phi\}^{(k-1)}$:

$$\begin{aligned} \mathcal{R}[\chi^{(k)}, \Phi^{(k)}; \delta\chi, \delta\Phi] &\approx \mathcal{R}[\chi^{(k-1)}, \Phi^{(k-1)}; \delta\chi, \delta\Phi] \\ &+ \frac{\partial \mathcal{R}[\chi^{(k-1)}, \Phi^{(k-1)}; \delta\chi, \delta\Phi]}{\partial \chi} \Delta\chi^{(k)} + \frac{\partial \mathcal{R}[\chi^{(k-1)}, \Phi^{(k-1)}; \delta\chi, \delta\Phi]}{\partial \Phi} \Delta\Phi^{(k)} = 0, \end{aligned} \quad (47)$$

leading to an algebraic system of equations for $\{\Delta\chi, \Delta\Phi\}^{(k)}$ of the form

$$\begin{bmatrix} \mathbf{H}_{\chi\chi} & \mathbf{H}_{\chi\Phi} \\ \mathbf{H}_{\Phi\chi} & \mathbf{H}_{\Phi\Phi} \end{bmatrix}^{(k-1)} \cdot \begin{bmatrix} \Delta\chi \\ \Delta\Phi \end{bmatrix}^{(k)} = - \begin{bmatrix} \mathbf{R}_\chi \\ \mathbf{R}_\Phi \end{bmatrix}^{(k-1)}, \quad (48)$$

given $\{\chi, \Phi\}^{(k-1)}$ at the previous iteration. The explicit form of the variations of the residual \mathcal{R} can be found in [Appendix B](#).

Once $\{\Delta\chi, \Delta\Phi\}^{(k)}$ are found, we compute the *modified* increments of the solution at the k -th iteration, namely $\{\widehat{\Delta\chi}, \widehat{\Delta\Phi}\}^{(k)}$, by ensuring that the total increment *i)* leads to an enthalpy decrease along χ , *ii)* leads to an enthalpy increase along Φ , and *iii)* has a predefined maximum norm $\gamma_{\max} \in \mathbb{R}^+$. The first two conditions are required in accordance to the variational principle in Eq. (32), whereas the latter is just a numerical requirement to avoid too large increments of the solution at each iteration. To formulate those conditions mathematically, let us recast the variational principle in Eq. (32) as

$$\widehat{\Phi}(\chi) := \operatorname{argmax}_{\Phi \in \mathcal{P}} (\Pi[\chi, \Phi]); \quad (49a)$$

$$\chi^* = \operatorname{argmin}_{\chi \in \mathcal{X}} (\widehat{\Pi}[\chi]), \quad \text{with} \quad \widehat{\Pi}[\chi] := \Pi[\chi, \widehat{\Phi}(\chi)]; \quad (49b)$$

$$\Phi^* = \widehat{\Phi}(\chi^*). \quad (49c)$$

Numerically, Eq. (49) is equivalent to solving two linear systems consecutively, constructed from Eq. (47) by writing $\Delta\Phi^{(k)}$ as a function of $\Delta\chi^{(k)}$, as follows:

$$\widehat{\mathbf{H}}_{\chi\chi}^{(k-1)} \cdot \Delta\chi^{(k)} = - \widehat{\mathbf{R}}_\chi^{(k-1)} \quad \text{with} \quad \begin{cases} \widehat{\mathbf{H}}_{\chi\chi}^{(k-1)} := \mathbf{H}_{\chi\chi}^{(k-1)} - \mathbf{H}_{\chi\Phi}^{(k-1)} \cdot \mathbf{H}_{\Phi\Phi}^{-1 (k-1)} \cdot \mathbf{H}_{\Phi\chi}^{(k-1)} \\ \widehat{\mathbf{R}}_\chi^{(k-1)} := \mathbf{R}_\chi^{(k-1)} - \mathbf{H}_{\chi\Phi}^{(k-1)} \cdot \mathbf{H}_{\Phi\Phi}^{-1 (k-1)} \cdot \mathbf{R}_\Phi^{(k-1)} \end{cases}; \quad (50a)$$

$$\mathbf{H}_{\Phi\Phi}^{(k-1)} \cdot \Delta\Phi^{(k)} = - \widehat{\mathbf{R}}_\Phi^{(k-1)} \quad \text{with} \quad \widehat{\mathbf{R}}_\Phi^{(k-1)} := \mathbf{R}_\Phi^{(k-1)} + \mathbf{H}_{\Phi\chi}^{(k-1)} \cdot \Delta\chi^{(k)}. \quad (50b)$$

From Eq. (50) it is clear that the descent and ascent directions are respectively identified by $\widehat{\mathbf{R}}_\chi^{(k-1)}$ and $\widehat{\mathbf{R}}_\Phi^{(k-1)}$, i.e. the *modified* residuals which take into account the coupled nature of the enthalpy

potential. Therefore, the modified increments are computed as follows:

$$\alpha_{\chi}^{(k)} = \begin{cases} -1 & \text{if } \widehat{\mathbf{R}}_{\chi}^{(k-1)} \cdot \Delta\chi^{(k)} > 0, \\ +1 & \text{otherwise;} \end{cases} \quad (51a)$$

$$\alpha_{\Phi}^{(k)} = \begin{cases} -1 & \text{if } \widehat{\mathbf{R}}_{\Phi}^{(k-1)} \cdot \Delta\Phi^{(k)} < 0, \\ +1 & \text{otherwise;} \end{cases} \quad (51b)$$

$$\beta^{(k)} = \min \left\{ +1, \gamma_{\max} / \sqrt{\left\| \frac{\Delta\chi^{(k)}}{\chi_0} \right\|^2 + \left\| \frac{\Delta\Phi^{(k)}}{\Phi_0} \right\|^2} \right\}; \quad (51c)$$

$$\overline{\Delta\chi}^{(k)} = \alpha_{\chi}^{(k)} \beta^{(k)} \Delta\chi^{(k)}; \quad (51d)$$

$$\overline{\Delta\Phi}^{(k)} = \alpha_{\Phi}^{(k)} \beta^{(k)} \Delta\Phi^{(k)}; \quad (51e)$$

with χ_0 and Φ_0 characteristic factors of the problem for displacement and potential. In practice, γ_{\max} is treated as an adaptive heuristic parameter, tunable for proper convergence.

Finally, the solution at the k -th iteration is updated with

$$\{\chi, \Phi\}^{(k)} = \{\chi, \Phi\}^{(k-1)} + \{\overline{\Delta\chi}, \overline{\Delta\Phi}\}^{(k)}. \quad (52)$$

The external loads are applied incrementally in a sequence of load steps, and the modified-step Newton-Raphson algorithm presented here is used to obtain converged solutions at every load step. Once convergence is reached, the stability of the solution is checked by assuring $\{\chi, \Phi\}^{(k)}$ is a saddle point in the enthalpy functional $\Pi[\chi, \Phi]$ in accordance to the variational principle in Eq. (32). By means of Eq. (49), stability of $\{\chi, \Phi\}^{(k)}$ is given by

$$\delta_{\chi}^2 \widehat{\Pi}[\chi^{(k)}; \Delta\chi; \Delta\chi] > 0 \quad \forall \Delta\chi \in \mathcal{X}, \quad (53a)$$

$$\delta_{\Phi}^2 \Pi[\chi^{(k)}, \Phi^{(k)}; \Delta\Phi; \Delta\Phi] < 0 \quad \forall \Delta\Phi \in \mathcal{P}. \quad (53b)$$

Numerically, Eq. (53) is met by checking the sign of the extremal eigenvalues λ of $\widehat{\mathbf{H}}_{\chi\chi}^{(k)}$ and $\mathbf{H}_{\Phi\Phi}^{(k)}$ as follows:

$$\lambda_{\min} \left[\widehat{\mathbf{H}}_{\chi\chi}^{(k)} \right] > 0, \quad \lambda_{\max} \left[\mathbf{H}_{\Phi\Phi}^{(k)} \right] < 0. \quad (54)$$

We recognize convergence to unstable solutions by the violation of Eq. (54). In such case, the solution $\{\chi, \Phi\}^{(k)}$ is slightly perturbed and the iterative algorithm is run again until a stable solution is found. In practice, we found that $\lambda_{\max} \left[\mathbf{H}_{\Phi\Phi}^{(k)} \right]$ remains always negative, and therefore the encountered instabilities are given by $\lambda_{\min} \left[\widehat{\mathbf{H}}_{\chi\chi}^{(k)} \right]$ becoming negative only (i.e. *geometrical* instabilities). The eigenvector associated to $\lambda_{\min} \left[\widehat{\mathbf{H}}_{\chi\chi}^{(k)} \right]$ is an appropriate direction for numerical perturbations on $\chi^{(k)}$ to reach stable solutions.

4 One-dimensional analytical models for flexoelectric rods undergoing large displacements and rotations

In this Section, we derive simplified closed-form solutions for planar bending and buckling of flexoelectric slender uniform rods undergoing large displacements and rotations under open circuit and close circuit conditions. A material point in the reference configuration is denoted by $\mathbf{X} = X_1 \mathbf{E}_1 + X_2 \mathbf{E}_3 + S \mathbf{E}_3$, where $\{\mathbf{E}_1, \mathbf{E}_2, \mathbf{E}_3\}$ is a global right-handed orthonormal basis of \mathbb{R}^3 , (X_1, X_2) denotes the coordinates of the undeformed cross-section and $X_3 = S$ is the Lagrangian coordinate along the undeformed arc-length, see Fig. 2. The rod is assumed to be extensible, and thus S is not arc-length of the deformed centerline, but unshearable, following the special Cosserat rod kinematics (Antman, 1995). We further assume that the cross-sections of the rod remain plane and rigid during the deformation. The corresponding deformation map can be defined as $\chi(X_1, X_2, S) = \mathbf{r}(S) + X_1 \mathbf{d}_1 + X_2 \mathbf{d}_2$, where $\mathbf{r}(S)$ is the deformed position of the centerline at $S \mathbf{E}_3$ and $(\mathbf{d}_1, \mathbf{d}_2)$ are the director vectors associated with the cross section. For planar bending (Fig. 2),

$$\mathbf{d}_1 = -\sin \theta \mathbf{E}_3 + \cos \theta \mathbf{E}_1, \quad (55)$$

$$\mathbf{d}_2 = \mathbf{E}_2, \quad (56)$$

where θ is the angle of deflection. The deformation gradient $F_{il} = \frac{\partial x_i}{\partial X_l}$ is obtained as

$$\frac{\partial \chi}{\partial X_1} = \mathbf{d}_1, \quad (57)$$

$$\frac{\partial \chi}{\partial X_2} = \mathbf{E}_2, \quad (58)$$

$$\frac{\partial \chi}{\partial S} = \mathbf{r}' + X_1 \mathbf{d}_1'. \quad (59)$$

where $\frac{d}{dS} = (\cdot)'$. Now, following Antman (1995), Gupta and Kumar (2017) we have

$$\mathbf{r}' = \nu_3 \mathbf{d}_3, \quad (60)$$

$$\mathbf{d}_1' = -\theta' \mathbf{d}_3, \quad (61)$$

where ν_3 is the stretch, and

$$\mathbf{d}_3 = \mathbf{d}_1 \times \mathbf{d}_2 = \cos \theta \mathbf{E}_3 + \sin \theta \mathbf{E}_1. \quad (62)$$

Thus, Eq. (59) becomes

$$\frac{\partial \chi}{\partial S} = (\nu_3 - X_1 \theta') \mathbf{d}_3, \quad (63)$$

the deformation gradient tensor can be written as

$$\mathbf{F} = \begin{bmatrix} \cos \theta & 0 & (\nu_3 - X_1 \theta') \sin \theta \\ 0 & 1 & 0 \\ -\sin \theta & 0 & (\nu_3 - X_1 \theta') \cos \theta \end{bmatrix}, \quad (64)$$

and the Green-Lagrange strain tensor as

$$\mathfrak{E} = \frac{1}{2} (\mathbf{F}^T \mathbf{F} - \mathbf{I}) = \frac{1}{2} \begin{bmatrix} 0 & 0 & 0 \\ 0 & 0 & 0 \\ 0 & 0 & (\nu_3 - X_1 \theta')^2 - 1 \end{bmatrix}. \quad (65)$$

We rewrite the only non-vanishing component of \mathfrak{E} as

$$2\mathfrak{E}_{33} = (\nu_3 - X_1 \theta')^2 - 1 \approx \nu_3^2 - 2X_1 \nu_3 \theta' - 1, \quad (66)$$

where the term $X_1^2 \theta'^2$ has been neglected for thin rods. Expanding ν_3 around $\nu_3 = 1$ in a Taylor series and neglecting higher order terms, since for a thin rod stretches are expected to be small, yields

$$\mathfrak{E}_{33} = \zeta - X_1 \theta', \quad (67)$$

where $\zeta = \nu_3 - 1$ is the axial strain. Retaining the above thin rod approximations and further assuming that the stretch and the curvature vary slowly along S , the dominant strain gradient component is

$$\widetilde{\mathfrak{E}}_{331} = -\theta'. \quad (68)$$

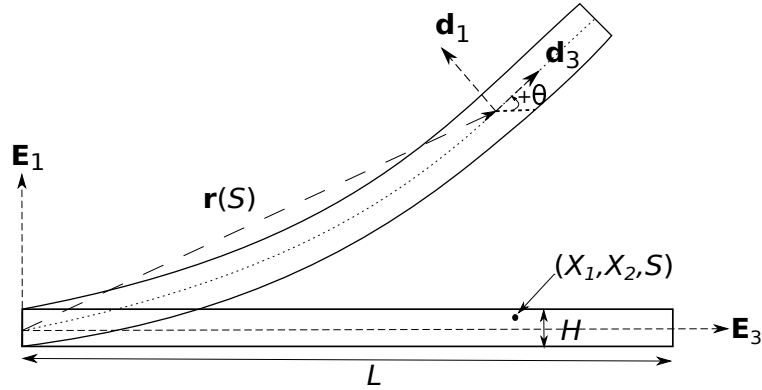


Figure 2: A typical schematic of deformed planar rod of length L and height H from its reference straight configuration. For upward bending, $\theta > 0$.

In the absence of body forces, neglecting strain gradient elasticity and the effect of E_3 , the equilibrium condition Eq. (33), reduces to

$$\int_0^L \left[\int_A \widehat{S}_{33} \delta \mathfrak{E}_{33} dA + \int_A \widetilde{S}_{331} \delta \widetilde{\mathfrak{E}}_{331} dA - \int_A D_1 \delta E_1 dA \right] dX_3 - \delta \hat{T} + \delta \hat{W} = 0. \quad (69)$$

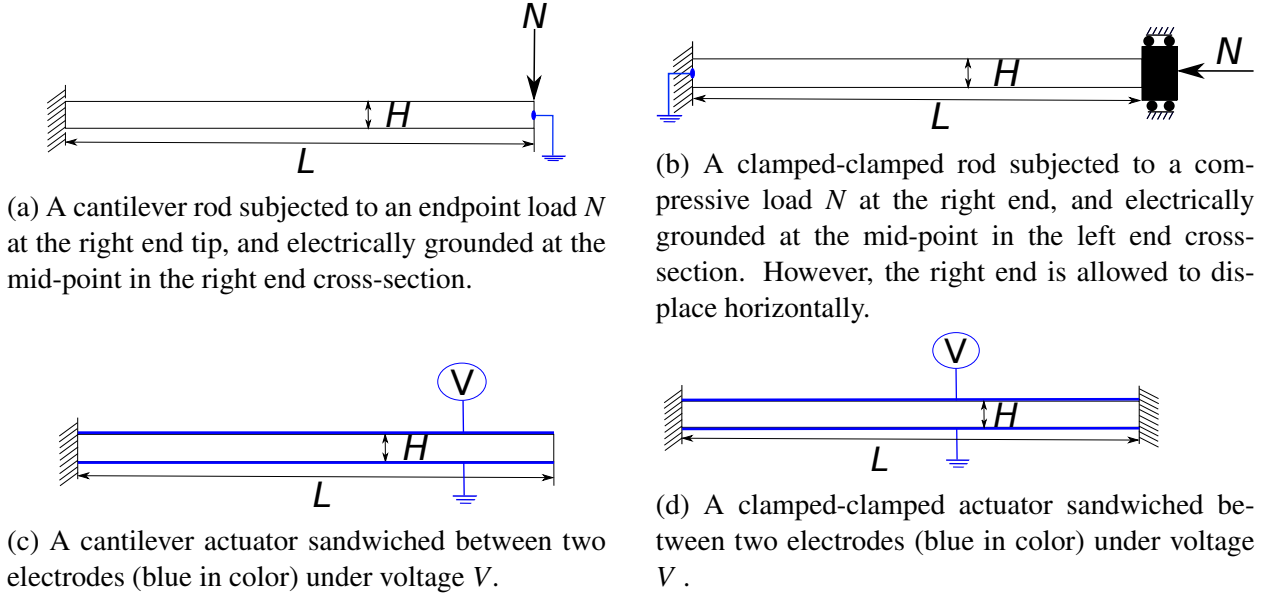


Figure 3: A schematic of flexoelectric rod under external mechanical load or external voltage.

where L is the undeformed length of the rod, A is area of the cross-section, and $\delta\hat{T}$ and $\delta\hat{W}$ are the variations of the external work done by mechanical tractions and surface charges. Since bending of slender rods can involve large displacements but typically small Lagrangian strains, all isotropic constitutive models are very close. For convenience, we consider the isotropic Kirchhoff-Saint-Venant model, requiring two elastic constants, here Young's modulus Y and Poisson's ratio ν , see Eq. (A.1). The flexoelectric tensor $\boldsymbol{\mu}$ is assumed to have cubic symmetry with three independent constants μ_L , μ_T and μ_S , namely the longitudinal, transversal and shear coefficients (Eq. (A.3)). We assume that all material properties are homogeneous in the cross-section.

Using Eqs. (67) and (68) in Eq. (69), the corresponding local stress, higher order stress and electric displacement relations in Eq. (36)-(38) reduce to

$$\widehat{S}_{33} = \bar{Y}(\zeta - X_1\theta') - (1 - \zeta + X_1\theta') \left(-E_1\mu_T\theta' + \frac{1}{2}\epsilon E_1^2 \right), \quad (70)$$

$$\widetilde{S}_{331} = -(1 + \zeta - X_1\theta') \mu_T E_1, \quad (71)$$

$$D_1 = (1 + \zeta - X_1\theta') (\epsilon E_1 - \mu_T\theta'), \quad (72)$$

with $\bar{Y} = Y(1 - \nu)/(1 + \nu)(1 - 2\nu)$. Note that in this reduced order theory, only transverse flexoelectricity is relevant.

4.1 Flexoelectric rod in open circuit under mechanical load

We consider now a flexoelectric rod in open circuit conditions, i.e. one of the rod end's is grounded and all other boundaries are free of surface charges, i.e. they satisfy that $\mathbf{D} \cdot \mathbf{n} = 0$, see Figs. 3a, 3b. Thus, at the top and bottom surfaces, the vertical electric displacement vanishes, $D_1 = 0$, and for thin rods it can be assumed to vanish within the cross-section as well (Majdoub et al., 2008, 2009, Liang et al., 2014). In this case, the vertical electric field can be computed from Eq. (72) as

$$E_1 = \frac{\mu_T}{\epsilon} \theta', \quad (73)$$

and then, Eqs. (70) and (71) reduce to

$$\widehat{S}_{33} = \bar{Y}(\zeta - X_1 \theta') + (1 - \zeta + X_1 \theta') \frac{\mu_T^2 \theta'^2}{2\epsilon}, \quad (74)$$

$$\widetilde{S}_{331} = -(1 - \zeta + X_1 \theta') \frac{\mu_T^2}{\epsilon} \theta'. \quad (75)$$

By substituting Eqs. (74) and (75) into Eq. (69), and using $\hat{W} = 0$ we obtain the following equilibrium condition

$$\int_0^L \left\{ \bar{Y}A \left[\zeta + \frac{1}{2}(1 - \zeta)\ell_\mu^2 \theta'^2 \right] \delta\zeta + \bar{Y} \left[I \left(1 - \frac{1}{2}\ell_\mu^2 \theta'^2 \right) + (1 - \zeta)\ell_\mu^2 A \right] \theta' \delta\theta' \right\} dX_3 - \delta\hat{T} = 0, \quad (76)$$

where $I = \int_A X_1^2 dA$ is the moment of inertia of the cross-section and $\ell_\mu = \mu_T / \sqrt{\bar{Y}\epsilon}$ is a lengthscale arising from transversal flexoelectricity. Since the stretch in thin rods is expected to be small, even if deformations are not, we can approximate $1 - \zeta \approx 1$ in Eq. (76), which yields

$$\int_0^L \left\{ \bar{Y}A \left[\zeta + \frac{1}{2}\ell_\mu^2 \theta'^2 \right] \delta\zeta + \bar{Y} \left[I \left(1 - \frac{1}{2}\ell_\mu^2 \theta'^2 \right) + \ell_\mu^2 A \right] \theta' \delta\theta' \right\} dX_3 - \delta\hat{T} = 0, \quad (77)$$

where we identify the axial force and the bending moment as

$$N = \bar{Y}A \left[\zeta + \frac{1}{2}\ell_\mu^2 \theta'^2 \right], \quad (78)$$

$$M = \bar{Y} \left[I - \frac{1}{2}\ell_\mu^2 \theta'^2 I + \ell_\mu^2 A \right] \theta'. \quad (79)$$

Interestingly, Eq. (77) points out the two main size-dependent effects of flexoelectricity. On one hand, flexoelectricity induces a positive size-dependent axial strain in the rod which depends quadratically on the flexural strain θ' . On the other hand, flexoelectricity modifies the effective bending stiffness by two size-dependent contributions of opposite sign. The first is a reduction in the rod's stiffness which depends quadratically on the flexural strain while the second makes the rod stiffer independent of deformation.

In order to evaluate the relative importance of the different contributions, let us consider a rectangular cross-section of unit width and thickness H , i.e. $I = H^3/12$ and $A = H$. The second and third contribution to the effective bending stiffness are comparable in magnitude for a radius of curvature $R = v_3/\theta' \approx H/5$, which is unphysically small. For reasonable radii of curvature, we expect $\frac{1}{2}\ell_\mu^2\theta'^2 I \ll \ell_\mu^2 A$, and thus Eq. (77) reduces to

$$\int_0^L \left[\bar{Y}A \left[\zeta + \frac{1}{2}\ell_\mu^2\theta'^2 \right] \delta\zeta + \bar{Y}I^{\text{eff}}\theta'\delta\theta' \right] dX_3 - \delta\hat{T} = 0, \quad (80)$$

with

$$I^{\text{eff}} = I + \ell_\mu^2 A. \quad (81)$$

Furthermore, the values of ℓ_μ for typical flexoelectric polymers are in the order of 1 – 10 nm (Chu and Salem, 2012, Zhang et al., 2015, Zhou et al., 2017). The minimum radius of curvature for a rectangular cross-section is $R = H/2$, which implies that the maximum flexoelectrically-induced axial strain is approximately $2\ell_\mu^2/H^2$, in the order of 10^{-3} for a $H = 100\text{nm}$ thick rod. Thus, we expect the flexoelectrically-induced axial strain to be small, as well as ζ . This is later verified in the numerical examples in Section 5.1, with ζ in the order of 10^{-4} for a $H = 100\text{nm}$ thick rod.

Keeping nevertheless the full axial strain $\zeta + \ell_\mu^2\theta'^2/2$, we consider now a flexoelectric cantilever rod subjected to a point load $\mathbf{N} = N_1\mathbf{E}_1 + N_3\mathbf{E}_3$ on one of its ends, Figs. 3a, 3b. The work done by the external force is

$$\hat{T} = \mathbf{N} \cdot \mathbf{r}(L) = \mathbf{N} \cdot \int_0^L (1 + \zeta) \mathbf{d}_3(S) dS = \int_0^L (1 + \zeta) (N_1 \sin \theta + N_3 \cos \theta) dS, \quad (82)$$

where we have used Eq. (60). Substituting the first variation of Eq. (82) in Eq. (80), and assuming that the stretch is small, i.e. $1 + \zeta \approx 1$ yields

$$\begin{aligned} \int_0^L \left[\bar{Y}A \left[\zeta + \frac{1}{2}\ell_\mu^2\theta'^2 \right] \delta\zeta + \bar{Y}I^{\text{eff}}\theta'\delta\theta' \right] dS \\ = \int_0^L [(N_1 \sin \theta + N_3 \cos \theta) \delta\zeta + (N_1 \cos \theta - N_3 \sin \theta) \delta\theta] dS. \end{aligned} \quad (83)$$

Upon integration by parts, Eq. (83) becomes

$$\begin{aligned} \int_0^L \left[\bar{Y}A \delta \left[\zeta + \frac{1}{2}\ell_\mu^2\theta'^2 \right] - \bar{Y}I^{\text{eff}}\theta''\delta\theta \right] dS + \bar{Y}I^{\text{eff}}\theta'\delta\theta \Big|_0^L \\ = \int_0^L [(N_1 \sin \theta + N_3 \cos \theta) \delta\zeta + (N_1 \cos \theta - N_3 \sin \theta) \delta\theta] dS, \end{aligned} \quad (84)$$

from where the Euler-Lagrange equations can be derived for all admissible $\delta\zeta$ and $\delta\theta$ as

$$\bar{Y}A\zeta + \frac{\bar{Y}A}{2}\ell_\mu^2\theta'^2 - N_1 \sin \theta - N_3 \cos \theta = 0, \quad (85a)$$

$$\bar{Y}I^{\text{eff}}\theta'' + N_1 \cos \theta - N_3 \sin \theta = 0, \quad (85b)$$

where we have assumed that the external force \mathbf{N} is known. Equations (85) form a system of two coupled equations for the two unknowns ζ and θ , where θ can be obtained from Eq. (85b) and used in Eq. (85a) to compute ζ . Note that Eq. (85b) corresponds to bending moment balance of a purely mechanical non-linear Kirchhoff rod with modified (larger) bending rigidity I^{eff} (Antman, 1995). This effective stiffness coincides with that identified by Majdoub et al. (2008, 2009), Liang et al. (2014) for linear flexoelectric rods. Equation (85b) can be rewritten in standard form as

$$\theta'' + \bar{\beta}^2 \mathbf{N} \cdot \mathbf{d}_1 = 0, \quad (86)$$

with $\bar{\beta}^{-2} = \bar{Y}I^{\text{eff}}$.

We derive next the solution for bending of a cantilever flexoelectric rod under a vertical point load, and buckling of a doubly clamped rod under axial compression, see Fig. 3a.

4.1.1 Bending of a flexoelectric cantilever under a vertical point load

We consider a cantilever flexoelectric rod subjected to a vertical force $\mathbf{N} = -N\mathbf{E}_1$, see Fig. 3a. In this case, Eq. (86) reduces to

$$\theta'' - \beta^2 \cos \theta = 0, \quad (87)$$

with $\beta^2 = \bar{\beta}^2 N$ and boundary conditions

$$\theta(0) = 0, \quad (88a)$$

$$\theta'(L) = 0. \quad (88b)$$

The solution to this problem was obtained by Bisshopp and Drucker (1945). As derived in detail in Appendix C, the vertical displacement of the tip is

$$r_1(L) = L + \frac{2}{\beta} \left[\tilde{E}(p, \psi_0) - \tilde{E}(p) \right], \quad (89)$$

where $\tilde{E}(p)$ and $\tilde{E}(p, \psi_0)$ are the complete and incomplete elliptical integrals of the second kind, respectively, see Eq. (C.12), with $p = \sqrt{(1 - \sin \theta_{\max})/2}$, and $1/\sin \psi_0 = \sqrt{1 - \sin \theta_{\max}}$, with $\theta_{\max} = \theta(L)$. For a given load N , θ_{\max} is obtained by the shooting method, using Eq. (C.9). Using Eqs. (85a) and (C.2), the axial strain can be computed as

$$\zeta(S) = -\frac{N}{\bar{Y}A} \sin \theta - \beta^2 \ell_\mu^2 (\sin \theta - \sin \theta_{\max}), \quad (90)$$

which attains its maximum value (in magnitude) at the free end

$$\zeta(L) = -\frac{N}{\bar{Y}A} \sin \theta_{\max}. \quad (91)$$

Note that for $N > 0$, the rod bends downwards ($\theta < 0$) while for $N < 0$, the rod bends upwards ($\theta > 0$) and thus in all cases $\zeta > 0$.

The electric field at the fixed end is (see Eq. (C.15))

$$E_1(0) = \frac{\mu_T}{\epsilon} \theta'(0) = -\frac{\mu_T}{\epsilon} \beta \sqrt{2 \sin |\theta^{\max}|} = -\ell_\mu \sqrt{\frac{2N}{\epsilon I^{\text{eff}}}} \sin |\theta^{\max}|. \quad (92)$$

In the limit case of small deflections, or small N , we recover the well-known flexoelectric theory relying on linear Euler-Bernoulli beams (Majdoub et al., 2008, 2009), yielding the vertical displacement at the free end and the curvature at the fixed end as

$$r_1(L) = -\frac{NL^3}{3\bar{Y}I^{\text{eff}}}, \quad (93)$$

$$\theta'(0) \approx -\frac{NL}{\bar{Y}I^{\text{eff}}}, \quad (94)$$

and thus the electric field at the fixed end for the linear Euler-Bernoulli beam is

$$E_1(0) = \frac{\mu_T}{\epsilon} \theta'(0) \approx -\frac{\mu_T NL}{\epsilon \bar{Y}I^{\text{eff}}}. \quad (95)$$

Interestingly, for a given rod of length L , with cross-section area A and moment of inertia I , the vertical electric field at the fixed end in Eq. (95) attains a maximum for

$$\mu_T^* = \sqrt{\epsilon \bar{Y} \frac{I}{A}}. \quad (96)$$

From a physical point of view, this maximum is a result of two competing effects of flexoelectricity. On one hand, flexoelectricity increases the bending rigidity of the rod by increasing the effective moment of inertia in $\ell_\mu^2 A \propto \mu_T^2$, see Eq. (81), and thus reduces the rod deflection, the curvature and the resulting vertical electric field. On the other hand, for a given curvature, the vertical electric field is proportional to μ_T . The maximum electric field at the fixed end for this optimum flexoelectric coefficient μ_T^* becomes

$$E_1^{\max}(0) = -\frac{NL}{2\sqrt{\epsilon \bar{Y} I A}}. \quad (97)$$

Similarly, for a given material with properties Y, ϵ , and μ_T , one can find an optimal design that maximizes the flexoelectric response. For instance, considering a rod with square/rectangular cross-section, the optimal thickness is

$$H^* = \mu_T \sqrt{\frac{12}{\bar{Y}\epsilon}} = 2\sqrt{3} \ell_\mu, \quad (98)$$

and the corresponding maximum vertical electric field at the fixed end for a rod with a unit width is

$$E_1^{\max}(0) = -\frac{\sqrt{\epsilon \bar{Y}} NL}{4\sqrt{3}\mu_T^2}. \quad (99)$$

4.1.2 Buckling of a flexoelectric rod under axial compression

We consider next an open-circuit flexoelectric rod clamped at the left end and with vertical displacement and rotation prevented at the right end, subjected to a compressive force $\mathbf{N} = -N\mathbf{E}_3$, see Fig. 3b. We examine the buckling critical load N_{cr} and the post-buckling behavior. In this case, the vertical reaction at the right end N_1 is unknown. Thus, the Euler-Lagrange Eqs. (85) have to be supplemented with the constraint of vanishing vertical displacements at the right end given by

$$0 = \mathbf{E}_1 \cdot \mathbf{r}(L) = \mathbf{E}_1 \cdot \int_0^L (1 + \zeta) \mathbf{d}_3(s) ds = \int_0^L (1 + \zeta) \sin \theta ds. \quad (100)$$

The bending moment balance Eq. (86) is written as

$$\theta'' + \beta^2 \sin \theta + N_1 \bar{\beta}^2 \cos \theta = 0, \quad (101)$$

with $\beta^2 = N/\bar{Y}I^{\text{eff}}$, subject to the boundary conditions

$$\theta(0) = 0, \quad (102a)$$

$$\theta(L) = 0. \quad (102b)$$

Since the expected lowest buckling mode is symmetric, the constraint in Eq. (100) is fulfilled by symmetry, and thus the reaction $N_1 = 0$, and Eq. (101) reduces to

$$\theta'' + \beta^2 \sin \theta = 0. \quad (103)$$

The expected lowest mode exhibits inflection points at $S = L/4$ and $S = 3L/4$, which require special attention (Lin and Chiao, 1998). Instead, we invoke symmetry considerations and avoid the inflection points by solving Eq. (103) over a quarter of the rod and replace Eq. (102b) with

$$\theta' \left(\frac{L}{4} \right) = 0. \quad (104)$$

After solving the BVP, see Appendix D for a detailed derivation, the vertical displacement and the vertical electric field at the center of the rod for upward buckling are,

$$r_1 \left(\frac{L}{2} \right) = \frac{2}{\beta} \sqrt{2(1 - \cos \theta^{\max})}, \quad (105a)$$

$$E_1 \left(\frac{L}{2} \right) = -\frac{\mu_T}{\epsilon} \sqrt{\frac{2N(1 - \cos \theta^{\max})}{\bar{Y}I^{\text{eff}}}}. \quad (105b)$$

where $\theta^{\max} = \theta(L/4)$ is computed for a given load N by the shooting method using Eq. (D.6). Since the right end of the rod is allowed to move horizontally, its length is assumed to remain unchanged and the stretch is $\nu_3 \approx 1$.

The post buckling load can be determined as

$$N = \frac{\beta^2}{\bar{\beta}^2} = 16F^2 \left(\sin \frac{\theta^{\max}}{2} \right) \frac{\bar{Y}I^{\text{eff}}}{L^2}, \quad (106)$$

where F is the complete elliptical integral of first kind, cf. Eq. (C.10), and we have used Eq. (D.6). By letting $\theta^{\max} \rightarrow 0$ in Eq. (106), the critical load for buckling is obtained as

$$N_{\text{cr}} = 4\pi^2 \frac{\bar{Y} I^{\text{eff}}}{L^2}, \quad (107)$$

which coincides with the buckling load for a linear flexoelectrically-stiffened Euler-Bernoulli beam with a modified bending stiffness (Timoshenko and Gere, 2009), see Eq. (81).

4.2 Flexoelectric rod actuator in closed circuit

We consider a flexoelectric rod in closed circuit, i.e. electrodes are attached to the top and bottom surfaces. Under actuation operation mode, i.e. the bottom electrode is grounded ($\phi = 0$), while a potential $\phi = V$ is applied to the top electrode, two setups are studied, bending of a cantilever, Fig. 3c, and buckling of a doubly clamped rod, Fig. 3d.

In these setups, neglecting the localized boundary effects at the ends of the rod, the non-vanishing electric field component is

$$E_1 = -\frac{V}{H}, \quad (108)$$

and then, Eqs. (70) – (72) reduce to

$$\widehat{S}_{33} = \bar{Y}(\zeta - X_1\theta') - (1 - \zeta + X_1\theta') \left(\frac{V}{H}\mu_T\theta' + \frac{\epsilon V^2}{2H^2} \right), \quad (109)$$

$$\widetilde{S}_{331} = (1 + \zeta - X_1\theta') \mu_T \frac{V}{H}, \quad (110)$$

$$D_1 = (1 + \zeta - X_1\theta') \left(-\epsilon \frac{V}{H} - \mu_T\theta' \right). \quad (111)$$

Hence, the balance law in Eq. (69) becomes

$$\begin{aligned} \int_0^L \left\{ \left[\left(\bar{Y} + \mu_T \frac{V}{H}\theta' + \frac{\epsilon V^2}{2H^2} \right) \zeta - \mu_T \frac{V}{H}\theta' - \frac{\epsilon V^2}{2H^2} \right] A \delta \zeta \right. \\ \left. + \left[\left(\bar{Y} + \mu_T \frac{V}{H}\theta' + \frac{\epsilon V^2}{2H^2} \right) I\theta' - (1 + \zeta) \mu_T \frac{V}{H} A \right] \delta \theta' \right\} ds - \delta \hat{T} = 0, \end{aligned} \quad (112)$$

where $\delta \hat{T}$ is given by Eq. (82) for an external force $\mathbf{N} = N_1 \mathbf{E}_1 + N_3 \mathbf{E}_3$ applied at the right end, and we have used $\delta E_1 = 0$, $\delta \hat{W} = 0$. Assuming again that the strain is small, integration by parts yields,

$$\begin{aligned} \int_0^L \left\{ \left[\left(\tilde{Y} + \mu_T \frac{V}{H}\theta' \right) \zeta - \mu_T \frac{V}{H}\theta' - \frac{\epsilon V^2}{2H^2} \right] A \delta \zeta - \left[\left(\tilde{Y} + \mu_T \frac{V}{H}\theta' \right) I\theta' - (1 + \zeta) \mu_T \frac{V}{H} A \right]' \delta \theta \right\} ds - \delta \hat{T} \\ = - \left[\left(\tilde{Y} + \mu_T \frac{V}{H}\theta' \right) I\theta' - (1 + \zeta) \mu_T \frac{V}{H} A \right] \delta \theta \Big|_{\theta(0)}^{\theta(L)}, \end{aligned} \quad (113)$$

where we have defined an effective Young's modulus modified by electrostriction as

$$\tilde{Y} = \bar{Y} + \frac{\epsilon V^2}{2H^2}. \quad (114)$$

4.2.1 Bending of a flexoelectric cantilever under applied voltage

We consider next a flexoelectric cantilever rod sandwiched between two electrodes as depicted in Fig. 3c. In this case, there are no applied mechanical loads and there is no kinematical constraint at the right end, and thus $\mathbf{N} = \mathbf{0}$. The Euler-Lagrange equations are identified as

$$\left(\tilde{Y} + \mu_T \frac{V}{H} \theta'\right) \zeta - \mu_T \frac{V}{H} \theta' - \frac{\epsilon V^2}{2H^2} = 0, \quad (115a)$$

$$\left[\left(\tilde{Y} + \mu_T \frac{V}{H} \theta'\right) I \theta' - (1 + \zeta) \mu_T \frac{V}{H} A\right]' = 0, \quad (115b)$$

Equation (115a) yields

$$\zeta = \frac{\mu_T \frac{V}{H} \theta' + \frac{\epsilon V^2}{2H^2}}{\tilde{Y} + \mu_T \frac{V}{H} \theta'} \approx \frac{\epsilon V^2}{2H^2 \tilde{Y}} + \frac{\mu_T V}{\tilde{Y} H} \left(1 - \frac{\epsilon V^2}{2\tilde{Y} H^2}\right) \theta', \quad (116)$$

where we have expanded ζ in a Taylor series around $\theta' = 0$ and have neglected the higher order terms, thereby assuming that the flexural strain is small. Replacing Eq. (116) in Eq. (115b) leads to

$$\left[\tilde{Y} \left(I - \frac{\mu_T^2 A V^2}{\tilde{Y}^2 H^2} \left(1 - \frac{\epsilon V^2}{2\tilde{Y} H^2}\right)\right) \theta' - \mu_T \frac{V}{H} A \left(1 + \frac{\epsilon V^2}{2\tilde{Y} H^2}\right)\right]' = 0. \quad (117)$$

By defining, an effective moment of inertia modified by flexoelectricity and electrostriction as

$$\tilde{I} = I - \frac{\mu_T^2 A V^2}{\tilde{Y}^2 H^2} \left(1 - \frac{\epsilon V^2}{2\tilde{Y} H^2}\right), \quad (118)$$

and an effective cross-section area modified by electrostriction as

$$\tilde{A} = A \left(1 + \frac{\epsilon V^2}{2\tilde{Y} H^2}\right), \quad (119)$$

Eq. (117) reduces to

$$\left[\tilde{Y} \tilde{I} \theta' - \mu_T \frac{V}{H} \tilde{A}\right]' = 0. \quad (120)$$

Equation (120) implies that the flexural strain θ' is uniform along s . By Eq. (113), the corresponding boundary conditions are

$$\theta(0) = 0, \quad (121)$$

$$\tilde{Y} \tilde{I} \theta'(L) - \mu_T \frac{V}{H} \tilde{A} = 0. \quad (122)$$

The resulting uniform flexural strain in this case is

$$\theta' = \theta'(L) = \mu_T \frac{V}{H} \frac{\tilde{A}}{\tilde{Y} \tilde{I}}, \quad (123)$$

which agrees with the expression given in [Bursian and Trunov \(1974\)](#) for a linear flexoelectric rod by replacing the effective quantities $(\tilde{Y}, \tilde{I}, \tilde{A})$ by the nominal ones (\bar{Y}, I, A) . From Eq. (116) the axial strain is obtained as

$$\zeta = \mu_T^2 \frac{\tilde{A}}{\tilde{Y}^2 \tilde{I}} \frac{V^2}{H^2} \left(1 - \frac{\epsilon V^2}{2 \tilde{Y} H^2} \right) + \frac{\epsilon V^2}{2 H^2 \tilde{Y}}. \quad (124)$$

We now examine Eqs. (123) and (124) by Taylor expansion of these expressions around $V/H = 0$ as

$$\theta' = \left(\frac{V}{H} \right) \frac{A \mu_T}{I \bar{Y}} + \left(\frac{V}{H} \right)^3 \frac{A^2 \mu_T^3}{I^2 \bar{Y}^3} + \mathcal{O} \left(\left(\frac{V}{H} \right)^5 \right), \quad (125a)$$

$$\begin{aligned} \zeta &= \frac{1}{2} \left(\frac{V}{H} \right)^2 \frac{\epsilon}{\bar{Y}} \left(1 + 2 \frac{A \ell_\mu^2}{I} \right) - \frac{1}{4} \left(\frac{V}{H} \right)^4 \left(\frac{\epsilon}{\bar{Y}} \right)^2 \left(1 + 4 \frac{A \ell_\mu^2}{I} - 4 \left(\frac{A \ell_\mu^2}{I} \right)^2 \right) + \mathcal{O} \left(\left(\frac{V}{H} \right)^6 \right) \\ &\approx \frac{1}{2} \left(\frac{V}{H} \right)^2 \frac{\epsilon}{\bar{Y}} - \frac{1}{4} \left(\frac{V}{H} \right)^4 \left(\frac{\epsilon}{\bar{Y}} \right)^2 + \mathcal{O} \left(\left(\frac{V}{H} \right)^6 \right) \end{aligned} \quad (125b)$$

According to Eq. (125a), under the application of a voltage V , the flexoelectric cantilever bends upwards for $V > 0$ and downwards for $V < 0$ due to the positive flexoelectric coupling, and elongates regardless of the sign of V , due to both flexoelectricity and electrostriction from Eq. (125b). However, the contribution of the flexoelectric effect on the axial strain is negligible as for typical flexoelectric elastomers $A \ell_\mu^2 / I \approx 10^{-2} \ll 1$ for a $H = 100\text{nm}$ thick rod, as previously argued in Section 4.1.

Finally, keeping only the leading order terms, the curvature of the rod is obtained from Eqs. (125) as

$$\frac{1}{R} = \frac{\theta'}{(1 + \zeta)} \approx \mu_T \frac{A}{I \bar{Y}} \frac{V}{H}. \quad (126)$$

Integrating θ from Eq. (126) and accounting for the clamping condition Eq. (121), we have

$$\theta(S) = (1 + \zeta) \mu_T \frac{A}{I \bar{Y}} \frac{V}{H} S. \quad (127)$$

Finally, the vertical deflection at the free end can be evaluated as

$$\begin{aligned} r_1(L) &= \int_0^L (1 + \zeta) \sin \theta \, dS = (1 + \zeta) \int_0^L \sin \left((1 + \zeta) \mu_T \frac{A}{I \bar{Y}} \frac{V}{H} S \right) dS \\ &= \frac{\tilde{Y} I}{\mu_T A} \frac{H}{V} \left[1 - \cos \left((1 + \zeta) \mu_T \frac{A L}{I \bar{Y}} \frac{V}{H} \right) \right] \approx \frac{\tilde{Y} I}{\mu_T A} \frac{H}{V} \left[1 - \cos \left(\mu_T \frac{A L}{I \bar{Y}} \frac{V}{H} \right) \right]. \end{aligned} \quad (128)$$

4.2.2 Buckling of a doubly-clamped flexoelectric rod under applied voltage

We consider now a doubly clamped flexoelectric rod in closed circuit conditions subjected to an external electrical bias V , Fig. 3d. Since as we have seen above, an applied bias leads to an elongation of the rod, if axially constrained this should lead to buckling, and hence here we study the critical buckling load V_{cr} and the post-buckling behavior. Similarly to Section 4.1.2, the kinematic constraints of vanishing vertical and horizontal displacements at the right end, give rise to a reaction force at the right end $\mathbf{N} = N_1 \mathbf{E}_1 + N_3 \mathbf{E}_3$, where now N_1 and N_3 are unknown quantities. Since the expected lowest buckling mode is symmetric, the vertical displacement at the right end vanishes by symmetry and thus $N_1 = 0$. Hence, Eq. (82) reduces to

$$\hat{T} = \int_0^L (1 + \zeta) N_3 \cos \theta \, dS, \quad (129)$$

and its variation is

$$\delta \hat{T} = \int_0^L [N_3 \cos \theta \, \delta \zeta - (1 + \zeta) N_3 \sin \theta \, \delta \theta] \, dS. \quad (130)$$

Replacing Eq. (130) in Eq. (113), the Euler-Lagrange equations are derived as

$$\left(\tilde{Y} + \mu_T \frac{V}{H} \theta' \right) A \zeta - \mu_T A \frac{V}{H} \theta' - \frac{\epsilon V^2}{2H^2} A - N_3 \cos \theta = 0, \quad (131a)$$

$$\left[\left(\tilde{Y} + \mu_T \frac{V}{H} \theta' \right) I \theta' - (1 + \zeta) \mu_T \frac{V}{H} A \right]' - (1 + \zeta) N_3 \sin \theta = 0, \quad (131b)$$

and the constraint of vanishing horizontal displacement at the right end is

$$\mathbf{E}_3 \cdot \mathbf{r}(L) - L = \mathbf{E}_3 \cdot \int_0^L (1 + \zeta) \mathbf{d}_3(S) \, dS - L = \int_0^L (1 + \zeta) \cos \theta \, dS - L = 0. \quad (132)$$

The unknown reaction force magnitude N_3 is calculated by evaluating Eq. (131a) at the left end, with $\theta(0) = 0$, as

$$N_3 = \left(\tilde{Y} + \mu_T \frac{V}{H} \theta'|_0 \right) A \zeta|_0 - \mu_T A \frac{V}{H} \theta'|_0 - \frac{\epsilon V^2}{2H^2} A. \quad (133)$$

Furthermore, by assuming that the axial strain and all material parameters are uniform along S and neglecting the nonlinear term $2\mu_T \frac{V}{H} \theta' I \theta''$, Eq. (131b) reduces to

$$\tilde{Y} I \theta'' - (1 + \zeta) N_3 \sin \theta = 0. \quad (134)$$

Finally, substituting N_3 from Eq. (133), Eq. (134) simplifies to

$$\theta'' + (1 + \zeta) \tilde{\beta}^2 \sin \theta = 0, \quad (135)$$

with

$$\tilde{\beta}^2 = \frac{A}{\tilde{Y}I} \left(-\tilde{Y}\zeta + \frac{\epsilon V^2}{2H^2} + (1 - \zeta)\mu_T \frac{V}{H} \theta|_0 \right), \quad (136)$$

and subject to the boundary conditions

$$\theta(0) = 0, \quad (137a)$$

$$\theta(L) = 0. \quad (137b)$$

Similarly to the problem in Section 4.1.2, the expected lowest mode exhibits inflection points at $S = L/4$ and $S = 3L/4$. To avoid having to deal with them, we consider only a quarter of the rod and replace Eq. (137b) with

$$\theta' \left(\frac{L}{4} \right) = 0, \quad (138)$$

After solution of the above BVP, see Appendix E for a detailed derivation, the vertical displacement at the center of the rod is obtained as

$$r_1 \left(\frac{L}{2} \right) = -\frac{4\sqrt{1+\zeta}}{\tilde{\beta}} \sin \frac{\theta^{\max}}{2}, \quad (139)$$

where $\theta^{\max} = \theta(L/4)$, and $\tilde{\beta}$ and ζ are computed from Eqs. (E.3) and (E.5) in terms of θ^{\max} . The curvature at the left end is

$$\theta'(0) = \tilde{\beta} \sqrt{2(1+\zeta)(1-\cos \theta^{\max})}. \quad (140)$$

Finally, using Eq. (136) and (140), the postbuckling voltage can be obtained as

$$V = \frac{H\sqrt{2\tilde{Y}/\epsilon}}{(1-\zeta) - \tilde{\beta}^2 I/A} \left(\sqrt{(\tilde{\beta}^2(\zeta+1)(\zeta-1)^2 \ell_\mu^2 (1-\cos \theta^{\max}) - ((\zeta-1) + \tilde{\beta}^2 I/A)(\zeta + \tilde{\beta}^2 I/A))} \right. \\ \left. + (\zeta-1)\tilde{\beta} \ell_\mu \sqrt{(\zeta+1)(1-\cos \theta^{\max})} \right) \quad (141)$$

The critical buckling voltage is determined from Eq. (141) in the limit $\theta^{\max} \rightarrow 0$ as

$$V_{\text{cr}} = \frac{2\pi H}{L} \sqrt{\frac{2\tilde{Y}}{\epsilon \left(\frac{A}{I} - \frac{4\pi^2}{L^2} \right)}}. \quad (142)$$

The critical electric field for a rectangular/square cross section becomes:

$$E_{\text{cr}} = \frac{2\pi}{L} \sqrt{\frac{2\tilde{Y}}{\epsilon \left(\frac{12}{H^2} - \frac{4\pi^2}{L^2} \right)}} = \left(\frac{H}{L} \right) \sqrt{\frac{2\tilde{Y}}{\epsilon \left(\frac{3}{\pi^2} - \left(\frac{H}{L} \right)^2 \right)}}, \quad (143)$$

and for slender rods, the Taylor approximation around $H/L \rightarrow 0$ provides

$$E_{\text{cr}} \approx \left(\frac{H}{L} \right) \pi \sqrt{\frac{2\tilde{Y}}{3\epsilon}}. \quad (144)$$

5 Numerical examples for general nonlinear flexoelectric rod problems

In this Section, we present numerical results of our general nonlinear model of flexoelectricity for bending and buckling of flexoelectric rods, both in open-circuit and in closed-circuit conditions. We compare these results with the solutions of the 1D nonlinear analytical model for rods developed in Section 4 and its linearized Euler-Bernoulli (E-B) counterpart, by considering material parameters to match the assumptions of these models. This comparison allows us to validate our computational approach. We then explore more general flexoelectric problems and establish the limits of the simplified 1D flexoelectric rod models.

To model standard elasticity, we consider isotropic hyperelastic potentials, either Saint-VenantKirchhoff (Eq. (A.1)) or Neo-Hookean (Eq. (A.2)) models, requiring two elastic constants, here Young's modulus Y and Poisson's ratio ν . Strain-gradient elasticity is modeled by the analogous isotropic hyperelastic Saint-VenantKirchhoff law (Eq. (A.4)), which additionally depends on the characteristic length scale ℓ . The flexoelectric tensor $\boldsymbol{\mu}$ is assumed to have cubic symmetry with three independent constants μ_L , μ_T and μ_S , namely the longitudinal, transversal and shear coefficients (Eq. (A.3)). Isotropic flexoelectricity tensor is just a particular case with only two independent parameters, with $2\mu_S = \mu_L - \mu_T$.

The dielectric strength (i.e. maximum electric field magnitude that a dielectric can sustain before electric breakdown occurs) is typically around $1 - 100\text{V}/\mu\text{m}$ (Liu, 2014). Here, for simplicity, electrical breakdown is neglected, i.e. we assume an infinite dielectric strength in all the examples. In all simulations, we consider a cubic ($p = 3$) spline mesh with square cells of size $h = H/10$, being H the thickness of the rod.

5.1 Bending of open-circuit flexoelectric cantilever under a vertical point load

We consider here a flexoelectric cantilever rod under bending by a vertical point load in an open circuit configuration with the mechanically free end electrically grounded, cf. Fig. 3a. Young's modulus is chosen as $Y = 1.725\text{GPa}$ and the dielectric permittivity as $\epsilon = 0.092\text{nJ}/\text{V}^2\text{m}$, which correspond to polyvinylidene fluoride (PVDF) (Chu and Salem, 2012, Zhang et al., 2016b, Zhou et al., 2017).

5.1.1 Validation

We first validate the full computational model in Section 2 and 3 against the 1D nonlinear model for flexoelectric rods presented in Section 4.1.1, and its linearized Euler-Bernoulli counterpart. For this, we choose a Saint-VenantKirchhoff mechanical constitutive law with $\nu = 0$ and material parameters consistent with the assumptions of the 1D reduced model, namely $\mu_L = \mu_S = 0$, $\ell = 0$. We consider a thickness $H = 100\text{nm}$ and a slenderness of $L/H \geq 20$. Fig. 4 collects all the validation results. Typical computational solutions are shown in Fig. 4a, where the electric

potential ϕ is plotted on the deformed configuration. These simulations highlight the very large deformations attained. In this figure, we show numerical calculations for a given force at the tip, and for several values of μ_T . As in the linear case (Majdoub et al., 2008, 2009) and as expected by the expression I^{eff} in the reduced theory, cf. Eq. (81), flexoelectricity leads to an effective stiffening of the system even though the elastic constants are kept fixed. As anticipated in Section 4.1.1 for the linearized Euler-Bernoulli beam, cf. Eq. (96), we find that also for the non-linear rod the maximum electric field generated at the clamping cross-section exhibits a maximum for an intermediate value of the flexoelectric constant. The existence of an optimal value of μ_T , for which the flexoelectric response is maximized results from the competition of the two conflicting effects of μ_T : (1) the stiffening and (2) the flexoelectric coupling. For small values of μ_T the structure is very compliant and larger strain gradients are attained but the generated field is small due to the small coupling, whereas for very large values of μ_T the flexoelectric coupling is large but the stiffer beam attains smaller deformations and thus smaller strain gradients.

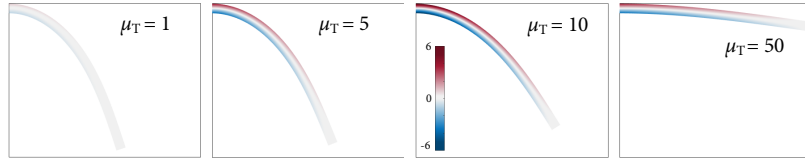
To further analyze these effects, we present in Fig. 4b the dependence of the cantilever rod vertical displacement at the tip on the endpoint load, and the vertical electric field on the clamped edge, for different values of transversal flexoelectric coefficient μ_T . The results for the tip displacement show *i*) the stiffening as μ_T increases, *ii*) the nonlinearity in the response of the system (particularly for the most deformable systems), *iii*) an excellent quantitative agreement with the nonlinear flexoelectric rod model given by the analytical expression in Eq. (89), and *iv*) an agreement with the linearized E-B model for small deformations, i.e. smaller loads or stiffer cantilevers (large values of μ_T). Similarly, we find an excellent agreement between the numerical simulations and the nonlinear rod model in the vertical electric field on the clamped end. Its behavior is nonlinear for large loads since the electric field is directly proportional to the curvature, cf. Eq. (73). The non-monotonicity in the maximum electric field as a function of μ_T discussed above is apparent from this plot. To further examine this point, we represent in Fig. 4c a contour plot showing the dependence of the vertical electric field at the clamped cross-section on μ_T and on the load. We find that the load for maximum electrical output depends on the value of the flexoelectric coupling in the nonlinear model, whereas it is independent of it according to the linearized E-B model, see Eq. (97).

Finally, we examine the effect of the slenderness on the load vs. deflection and the load vs. electric field curves for a given μ_T , see Fig. 4d. As the slenderness ratio increases, the rod becomes more flexible and therefore nonlinearity is stronger and manifests for smaller loads, with a larger overestimation of the vertical displacement by the linear E-B model. In contrast, the nonlinear 1D rod model closely follows our simulations even deep into the nonlinear regime.

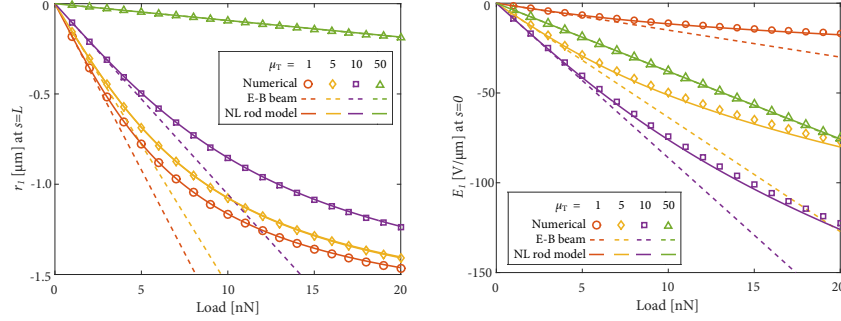
5.1.2 General flexoelectric problem

We investigate now more general flexoelectric conditions beyond the restrictive assumptions of the reduced model in Section 4.1.1. We consider an $L = 2\mu\text{m}$ by $H = 100\text{nm}$

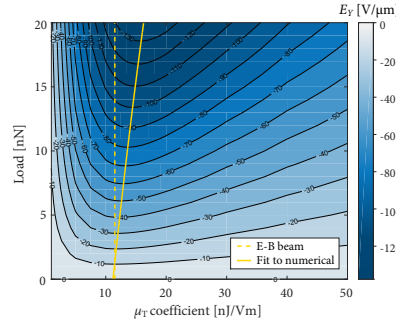
isotropic Neo-Hookean hyperelastic rod, cf. Eq. (A.2), augmented with strain gradient elasticity, with $\nu = 0.3$, $\ell = 0.1\ \mu\text{m}$ and varying flexoelectric constants.



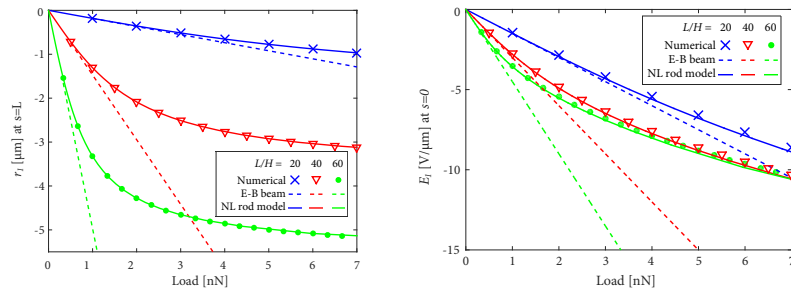
(a) Deformed shape and electric potential [V] distribution of cantilever rods of slenderness $L/H = 20$ under a point load of 20 nN, for different transversal flexoelectric coefficients μ_T .



(b) Bending of a cantilever rod of slenderness $L/H = 20$ with varying transversal flexoelectric coefficient μ_T . The left plot shows the vertical displacement at the loaded end, and the right one shows the vertical electric field at the fixed end.

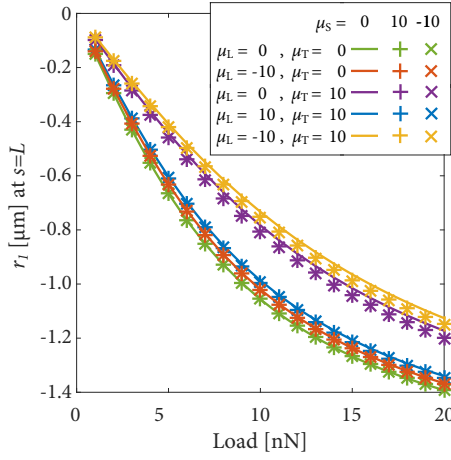


(c) Contour plot the vertical electric field E_l at the fixed end of the rod of $L/H = 20$ as a function of the applied load and the transversal flexoelectric coefficient μ_T .

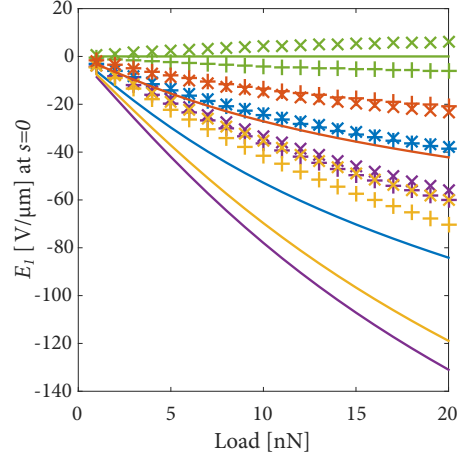


(d) Bending of a cantilever rod of $\mu_T = 1 \text{ nJ/Vm}$ with varying slenderness. The left panel shows the vertical displacement at the loaded end, and the right one shows the vertical electric field at the fixed end.

Figure 4: Validation results for bending of open-circuit flexoelectric cantilever in sensor mode. The transversal flexoelectric coefficient μ_T in the legends is expressed in $\text{nJ/Vm} = \text{nC/m}$.



(a) Vertical displacement at the loaded end.



(b) Vertical electric field at the fixed end.

Figure 5: Electromechanical response of Neo-Hookean cantilever flexoelectric sensor under bending, with different flexoelectric tensors (expressed in nJ/Vm).

Fig. 5 represents the electromechanical response of the open circuit cantilever rod under point load for varying flexoelectric constants $\mu_L, \mu_T, \mu_S = \{-10, 0, 10\}$ nJ/Vm. Fig. 5a shows the deflection r_1 of the loaded end, whereas Fig. 5b shows the vertical electric field E_1 at the clamped end. For the sake of brevity, some combinations of flexoelectric tensors are omitted, since we found that the responses are analogous to the ones of other combinations as follows:

$$r_1|_{\mu} = r_1|_{-\mu}; \quad (145a)$$

$$E_1|_{\mu} = -E_1|_{-\mu}. \quad (145b)$$

From Fig. 5a, it is clear that flexoelectricity is always increasing the bending stiffness of the rod. The largest stiffening is found with opposite μ_T and μ_L , followed by the case of vanishing μ_L . On the contrary, the simulations with $\mu_L \sim \mu_T$ and the ones with vanishing μ_T present a smaller stiffening. In all cases, the effect of the shear flexoelectric coefficient μ_S on bending stiffness is much smaller, and therefore less relevant.

Fig. 5b shows the electric response of the rod at the clamped tip, revealing that all three flexoelectric coefficients are relevant here. Within the studied range, a larger flexoelectricity-induced bending stiffness leads also to a larger electric field. However, in addition, the shear flexoelectric effect μ_S has a large influence on the electric field. In most cases, a non-vanishing μ_S leads to a substantial decrease in the reported electric field, which slightly depends also on the sign of μ_S . The only case in which a non-vanishing μ_S increases the electric field is the one where μ_S is the *only* non-vanishing flexoelectric coefficient.

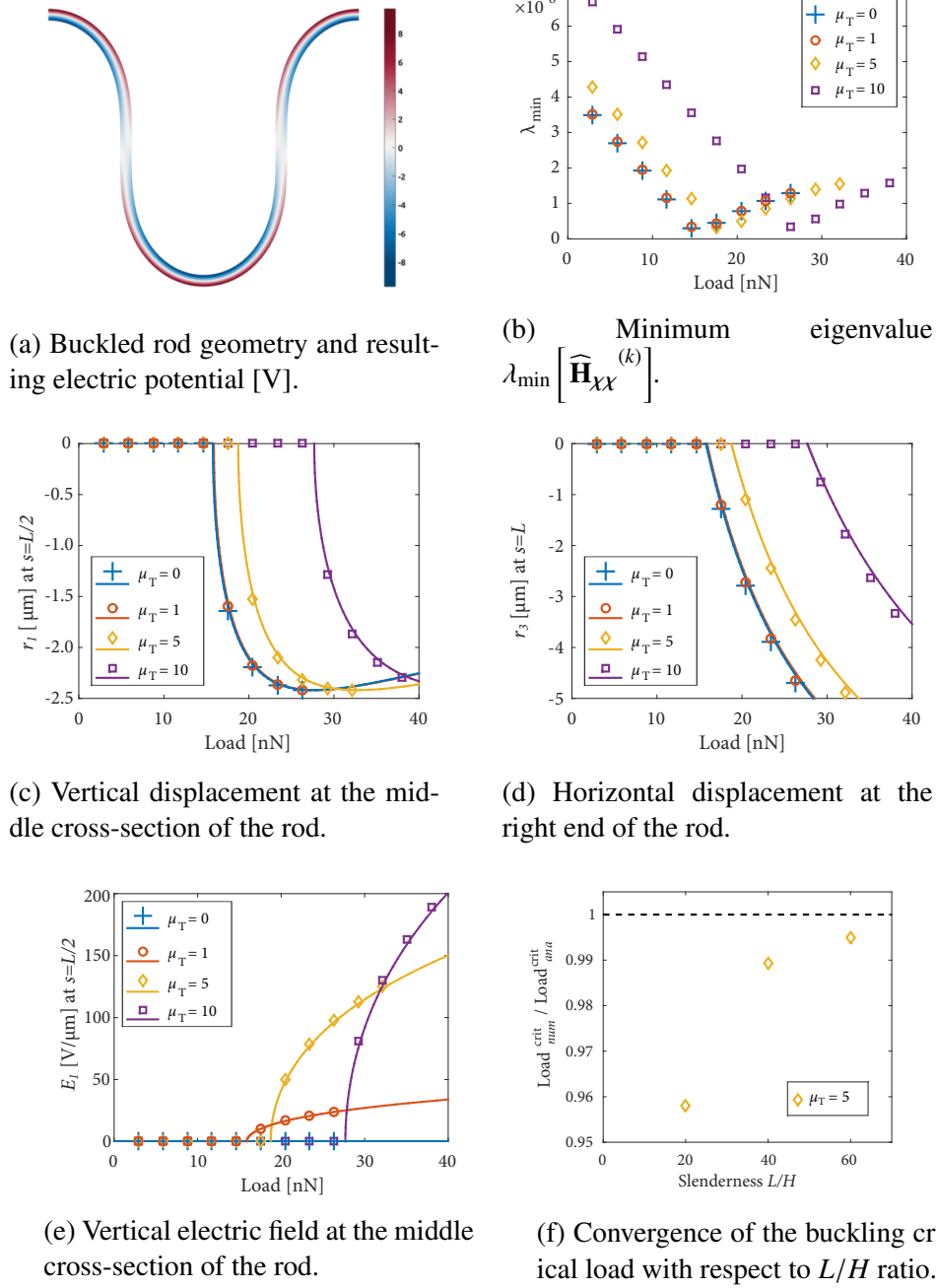


Figure 6: Force-controlled buckling of a flexoelectric rod of $L/H = 60$. Markers refer to the numerical implementation and solid lines refer to the analytical nonlinear model for rods. The transversal flexoelectric coefficient μ_T is expressed in nJ/Vm.

5.2 Buckling of open-circuit flexoelectric rod under mechanical load

We now compress a slender flexoelectric rod ($L = 6 \mu\text{m}$, $H = 100 \text{ nm}$) in open-circuit until buckling occurs, and also during the post-buckling stage. The left tip is clamped and a uniform horizontal load is applied on the right cross-section, which can only move uniformly in axial direction, i.e. vertical displacement and rotation of the right end are prevented (see Fig. 3b). We consider an isotropic Saint-VenantKirchhoff model with Young's modulus $Y = 1.725 \text{ GPa}$, dielectric permittivity $\epsilon = 0.092 \text{ nJ/V}^2\text{m}$ and different transversal flexoelectric coefficients: $\mu_T = \{0, 1, 5, 10\} \text{ nJ/Vm}$. The other material parameters are set to zero ($\nu = \mu_L = \mu_S = \ell = 0$).

As shown in Fig. 6, the numerical simulations and the analytical 1D model agree remarkably well. The highly nonlinear nature of the electromechanical system is clear in the responses reported in the post-buckling regime. Before buckling, the system is uniformly compressed and the flexoelectric effect is not present yet since the rod is not bent, and hence the electric response is zero. Once the rod has buckled (see Fig. 6a), the vertical displacement at $s = L/2$ (Fig. 6c) and the horizontal displacement at $s = L$ (Fig. 6d) suddenly deviate from zero and evolve nonlinearly with respect to the applied load. The flexoelectric effect arises due to the curvature induced by buckling, leading to a measurable electric field at $s = L/2$, which also evolves nonlinearly with applied load (Fig. 6e).

The role of the magnitude of the flexoelectric coefficient μ_T is twofold. On the one hand, the critical buckling load becomes larger with a larger μ_T coefficient, as suggested by the nonlinear rod model, cf. Eq. (107), for an effectively stiffer structure. Numerically, the precise value of the critical buckling load is identified by the load at which the eigenvalue $\lambda_{\min} \left[\widehat{\mathbf{H}}_{\chi\chi}^{(k)} \right]$ vanishes, as reported in Fig. 6b. On the other hand, the electric field at the post-buckling stage grows faster with a larger μ_T coefficient, which is also predicted by the nonlinear rod model, cf. Eq. (105b). Thus, the buckling-induced flexoelectric response is delayed but stronger when μ_T is larger.

We expect the agreement of the simplified rod model and the computational model to deteriorate for thicker rods, and thus the assumptions of the rod model loose validity. In Fig. 6f we show the effect of the finite thickness of the rod on the buckling critical load by plotting the value predicted by the computational model normalized by that estimated by the nonlinear rod model for different values of slenderness L/H . For all L/H values, the 1D nonlinear rod model overestimates the buckling load, as it provides as more constrained model. As expected, Fig. 6f shows that the buckling critical load computed with the 2D computational model converges towards the approximated value given by the 1D nonlinear rod model as the slenderness L/H increases and thus the 1D assumption is approached.

5.3 Bending of closed-circuit flexoelectric cantilever under electric actuation

We now consider a closed-circuit flexoelectric cantilever rod with Young's modulus $Y = 1.0 \text{ GPa}$, dielectric permittivity $\epsilon = 0.1 \text{ nJ/V}^2\text{m}$, and dimensions $L = 20 \mu\text{m}$, $H = 1 \mu\text{m}$, which rolls up into a circle upon electrical stimulus. The geometry and boundary conditions are depicted in Fig. 3c.

The left tip cross-section of the rod is clamped, while all other boundaries are traction-free. The electric potential at the top boundary is set to a certain non-zero value $\phi = V$, and the bottom boundary is grounded ($\phi = 0$). The voltage difference $\Delta\phi = V$ induces a transverse electric field across the rod thickness, cf. Eq. (108), which triggers the flexoelectric and electrostrictive effects, thereby generating a non-uniform strain that bends the rod, as shown in Fig. 8d. Depending on the sign of the applied electric field the cantilever will bend upwards or downwards. This bending actuator was first used by Bursian and Zaikovskii (1968) to experimentally demonstrate for the first time the flexoelectric effect, which had been predicted theoretically by Mashkevich and Tolpygo (1957).

5.3.1 Validation

Figure 7 shows the electromechanical response of an elastically isotropic Saint-VenantKirchhoff flexoelectric rod ($\nu = l = 0$) with the flexoelectric constants $\mu_T = 10\text{nJ/Vm}$, $\mu_L = \mu_S = 0$. The curvature $1/R$ (Fig. 7a) and the axial strain ζ (Fig. 7b) are captured very well by the closed-circuit flexoelectric rod model, where we have considered only the leading term in the expansions in Eq. (125), up to a relatively large value of applied voltage V . Beyond this limit, the small strains assumption of the 1D non-linear model loose validity. According to Eq. (125), the rod bends thanks to the flexoelectric coupling, and elongates mainly due to electrostriction, cf Section 4.2.1.

5.3.2 General flexoelectric problem

Since the curvature is found to be uniform, cf. Eq. (126), the rod forms an arc of a circle, cf. Fig. 8d. Thus, a natural question that arises is which set of flexoelectric parameters achieve a fully-closed circular shape more efficiently (i.e. with a lower applied voltage). To address this question, we

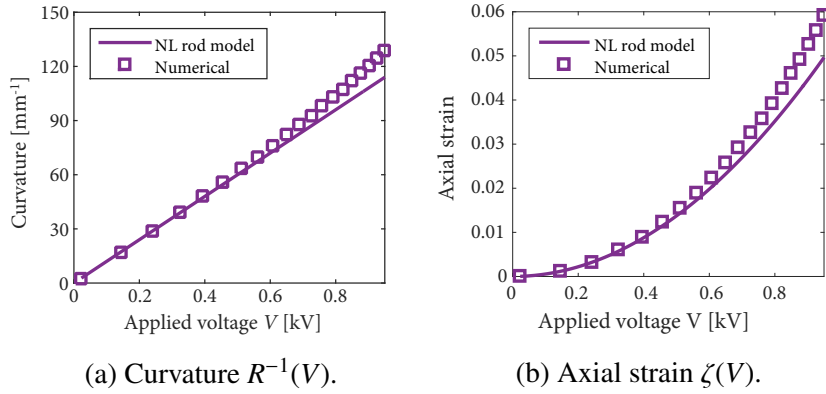


Figure 7: Actuation of Saint-VenantKirchhoff cantilever rod with transversal flexoelectric coefficient $\mu_T = 10\text{nJ/Vm}$. Numerically, the axial strain corresponds to the axial component of the Green-Lagrangian strain tensor (\mathcal{E}_{33}), whereas the value from the 1D model corresponds to its Taylor approximation in Eq. (67), evaluated at $X_1 = 0$.

consider an isotropic Neo-Hookean elastic (see Eq. (A.2)) rod with $\nu = 0.37$, $\ell = 0.03\mu\text{m}$ and varying flexoelectric constants. To quantify the curvature of the rod relative to the curvature of the closed circle, we define the normalized curvature $\overline{R^{-1}}(V) = R^{-1}(V)/R_o^{-1}(V)$, where $R_o^{-1}(V) = 2\pi/((1 + \zeta(V))L)$ is the curvature required to form a closed circular shape.

Figure 8 shows the evolution of $\zeta(V)$, $R^{-1}(V)$ and $\overline{R^{-1}}(V)$ for flexoelectric tensors with different combinations of longitudinal (μ_L), transversal (μ_T) and shear (μ_S) flexoelectric coefficients. The cases including a non-vanishing shear coefficient are omitted, since the results do not change significantly, even when μ_S is one order of magnitude larger than μ_L or μ_T . For the sake of brevity, the simulations (i) with negative applied electric voltage V , and (ii) yielding negative curvatures, are also omitted since the results are analogous to those simulations with (i) positive applied voltage and (ii) negative flexoelectric coefficients, respectively, as

$$\zeta(V)|_{\mu} = \zeta(-V)|_{\mu} = \zeta(V)|_{-\mu} = \zeta(-V)|_{-\mu}; \quad (146a)$$

$$R^{-1}(V)|_{\mu} = -R^{-1}(-V)|_{\mu} = -R^{-1}(V)|_{-\mu} = R^{-1}(-V)|_{-\mu}; \quad (146b)$$

$$\overline{R^{-1}}(V)|_{\mu} = -\overline{R^{-1}}(-V)|_{\mu} = -\overline{R^{-1}}(V)|_{-\mu} = \overline{R^{-1}}(-V)|_{-\mu}; \quad (146c)$$

in accordance with Eqs. (125a) and (126).

As expected, the axial strain of the rod (depicted in Fig. 8a) does not vary much with the different flexoelectric parameters, since it is mainly a consequence of electrostriction. The curvature (Fig. 8b), instead, varies significantly for the different combinations of flexoelectric parameters. The dominant parameter is the transversal flexoelectric coefficient μ_T which leads to positive curvature, as shown in case B. The longitudinal flexoelectric coefficient μ_L is also relevant and leads to negative curvature, as shown in case D. The largest response is found with positive μ_T and negative μ_L , as shown in case A. Finally, case C corresponds to positive μ_L and μ_T , and yields curvatures inbetween cases B (purely transversal μ) and D (purely longitudinal μ).

The normalized curvature is shown in Fig. 8c. For sufficiently large actuation, case A reaches $\overline{R^{-1}} > 1$, which indicates that the actuator rolls up forming a closed circle. This process is shown in Fig. 8d, where the deformed configuration and electric potential distribution within the rod is depicted at different applied voltages. We also show in Fig. 8e the resulting polarization field once the circle is formed, which remains normal to the bent rod.

5.4 Buckling of closed-circuit flexoelectric cantilever under electric actuation

In the previous example, the rod undergoes elongation upon electrical actuation mainly due to electrostriction. In this Section, we present a similar setup where the right tip is also clamped, as shown in Fig. 3d. In this case, an axial compressive force is expected at the clamped ends since the elongation of the rod is prevented. Restricting Eq. (133) in pre-buckling stage, the axial force grows quadratically with the applied voltage and, for a large enough applied (critical) voltage V_{cr} , cf. Eq. (143), a mechanical instability is reached, inducing buckling of the rod.

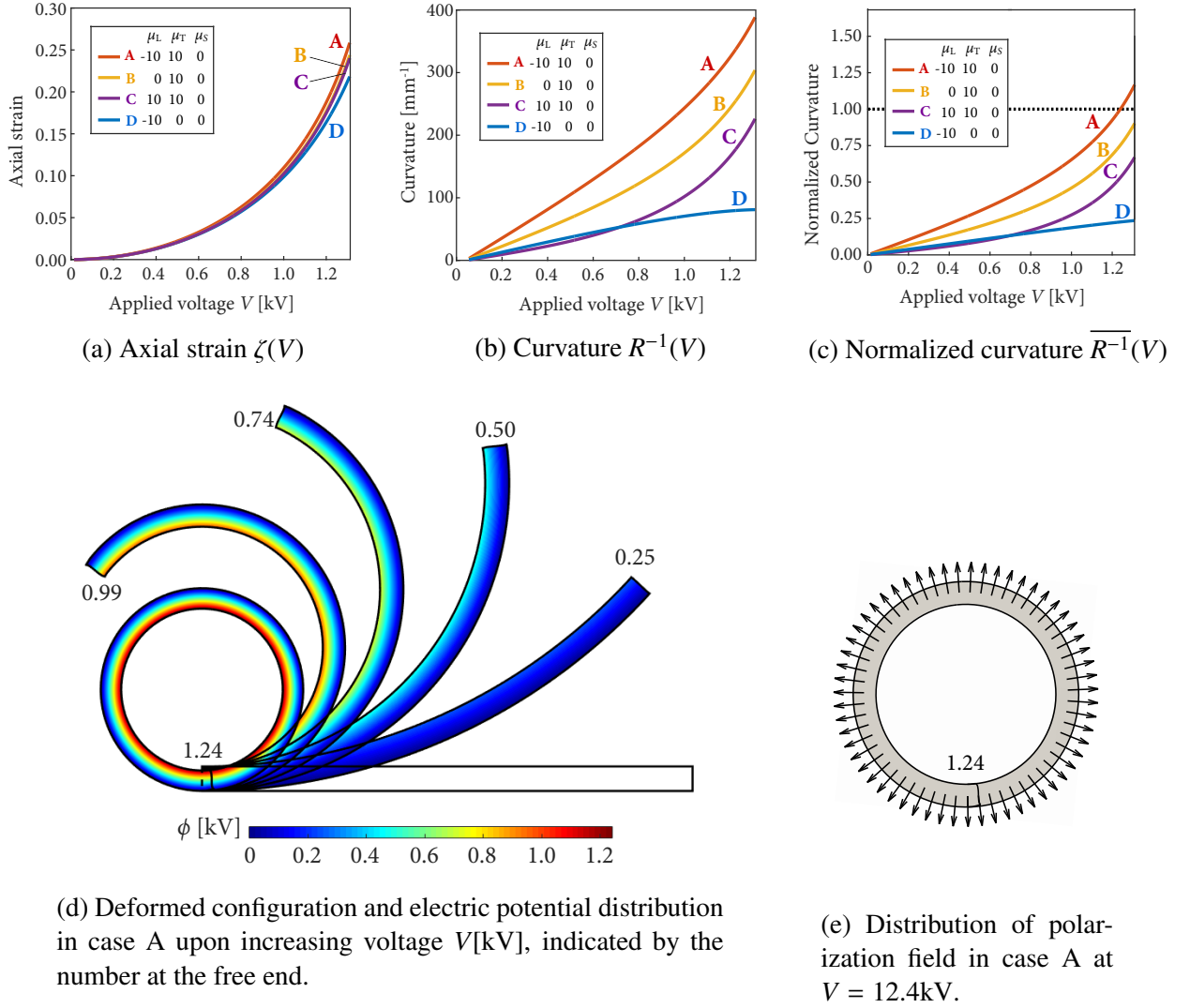
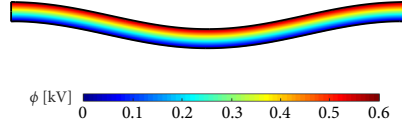
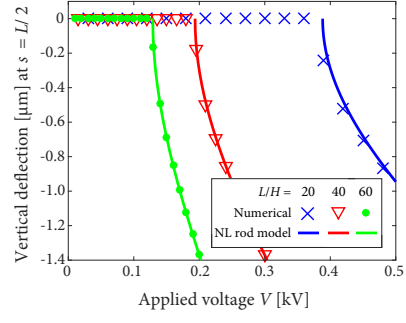


Figure 8: Actuation of Neo-Hookean cantilever rod with different flexoelectric tensors (expressed in nJ/Vm)

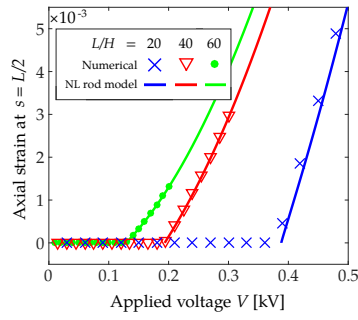
Figure 9 shows numerical simulations of a flexoelectric Saint-VenantKirchhoff rod ($\nu = \ell = 0$) of dimensions $L = 20\mu\text{m}$, $H = 1\mu\text{m}$, with Young's modulus $Y = 1.0\text{GPa}$, dielectric permittivity $\epsilon = 0.11\text{nJ/V}^2\text{m}$ and transversal flexoelectric coefficient $\mu_T = 10\text{nJ/Vm}$ ($\mu_L = \mu_S = 0$). The postbuckling configuration and the evolution of the maximum deflection and axial strain with respect to applied voltage are depicted in Fig. 9a-9c, showing an excellent match between the numerical results and the analytical expressions in Eq. (139), (141) and (E.5). The critical voltage at which the rod buckles (see Fig. 9d) matches also with the one predicted by the analytical 1D nonlinear model in Eq. (142), and the critical electric field (cf. Fig. 9e) is inversely proportional to the slenderness of the rod, as predicted in Eq. (144).



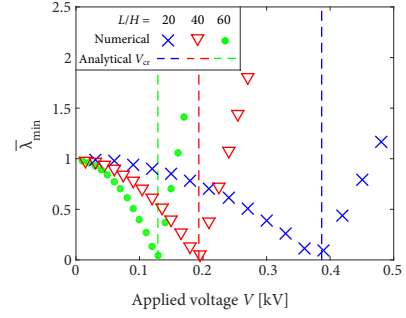
(a) Buckled shape and electric potential distribution of the $L/H = 20$ -slender rod upon electrical loading of 0.6kV.



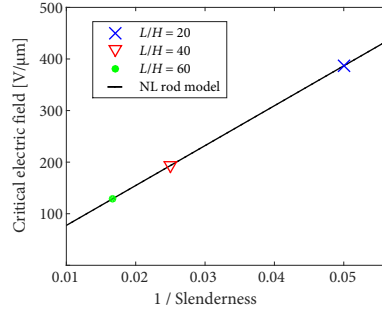
(b) Vertical deflection r_1 at the center of the rod.



(c) Axial strain as a function of slenderness.



(d) Normalized minimum eigenvalue $\lambda_{\min}[\widehat{\mathbf{H}}_{\chi\chi}^{(k)}]$ and critical voltage of analytical 1D model. $\bar{\lambda}_{\min} = \lambda_{\min}(n_{\text{DOF}}/n_0)^4$, where n_{DOF} is the number of degrees of freedom of each simulation, and $n_0 = 312$ is an arbitrary normalization constant, chosen such that $\bar{\lambda}_{\min}(0) \approx 1$.



(e) Critical electric field as a function of slenderness.

Figure 9: Actuation of Saint-VenantKirchhoff clamped-clamped rod with transversal flexoelectric coefficient $\mu_T = 10\text{nJ/Vm}$ and varying slenderness.

6 Conclusions and directions of future work

We have developed the material form of the balance equations for dielectric elastomers, including the flexoelectric effect. Unlike previously considered models of the flexoelectric coupling, here we formulate our model in terms polarization, strain gradients and flexocoupling tensor in a fully material frame. As a result, our formulation is objective by construction, and the flexocoupling tensor has the same symmetries as that used in linearized theories. After partial Legendre transform, the equations are written in terms of the electric potential and the displacement field as a fourth order unconstrained system of partial differential equations, which is convenient for finding numerical and analytical solutions. A numerical implementation of the theory is developed using open B-spline basis of sufficient smoothness on a uniform Cartesian grid, enabling robust simulations deep into the nonlinear regime, for very large deformations, and including mechanical instabilities (Yvonnet and Liu, 2017). On the other hand, analytical closed-form solutions are derived for open- and closed-circuit nonlinear extensible flexoelectric rods under bending and buckling. Direct comparison of this model with direct numerical simulations of the full model shows excellent agreement well into the nonlinear regime in conditions where the rod theory is expected to apply. The analytical rod theory serves both as a means of validation of our nonlinear simulations, and as fast and simple model to analyze and design nonlinear flexoelectric devices.

The current model could be easily extended in several ways. For instance, rather than homogeneous electric Neumann boundary conditions on the free surfaces, it may be more realistic to directly model the surrounding medium as a dielectric when considering soft materials materials with relatively low dielectric constant (Yvonnet and Liu, 2017, Thai et al., 2018). Our model can be extended to account for converse flexoelectricity (Lifshitz and Landau, 1984, Sharma et al., 2010, Landau and Lifshitz, 2013), for polarization gradient dielectricity (Mindlin, 1968), for material incompressibility, and coupled with flexible discretization methods, e.g. based on immersed boundaries (Codony et al., 2019), to model domains of general, and possibly complex, geometry that might enhance field gradients.

Acknowledgments

This work was supported by the Generalitat de Catalunya (ICREA Academia award for excellence in research to I.A., and Grant No. 2017-SGR-1278), and the European Research Council (StG-679451 to I.A.). CIMNE is recipient of a Severo Ochoa Award of Excellence from the MINECO.

Appendix A Material characterization

The material is fully characterized by specifying the elastic energy density $\Psi^{\text{Elast}}(\mathbf{C})$ and the material tensors of flexoelectricity $\boldsymbol{\mu}$ and strain gradient elasticity \mathbf{h} .

Isotropic Saint-VenantKirchhoff model.

It corresponds to the extension of the linear isotropic elastic material model to the non-linear regime, and depends on the Lamé parameters $\lambda = Y\nu/(1+\nu)(1-2\nu)$ and $\mu = Y/2(1+\nu)$ as follows:

$$\Psi^{\text{Elast}}(\mathbf{C}) = \frac{\lambda}{2} [\text{Tr}(\mathfrak{E})]^2 + \mu \text{Tr}(\mathfrak{E}^2), \quad (\text{A.1a})$$

$$\frac{\partial \Psi^{\text{Elast}}(\mathbf{C})}{\partial C_{IJ}} = \frac{\lambda}{2} [\text{Tr}(\mathfrak{E})] \delta_{IJ} + \mu \mathfrak{E}_{IJ}, \quad (\text{A.1b})$$

$$\frac{\partial^2 \Psi^{\text{Elast}}(\mathbf{C})}{\partial C_{IJ} \partial C_{KL}} = \frac{\lambda}{4} \delta_{IJ} \delta_{KL} + \frac{\mu}{2} \delta_{IK} \delta_{JL}. \quad (\text{A.1c})$$

Isotropic Neo-Hookean model

The Neo-Hookean model is adequate for describing nonlinear stress-strain behavior of cross-linked polymers at moderate strains. It is mathematically defined as

$$\Psi^{\text{Elast}}(\mathbf{C}) = \frac{\lambda}{2} [\log(J)]^2 + \frac{\mu}{2} [\text{Tr}(\mathbf{C}) - 2], \quad (\text{A.2a})$$

$$\frac{\partial \Psi^{\text{Elast}}(\mathbf{C})}{\partial C_{IJ}} = \frac{\lambda}{2} \log(J) C_{IJ}^{-1} + \frac{\mu}{2} (\delta_{IJ} - C_{IJ}^{-1}), \quad (\text{A.2b})$$

$$\frac{\partial^2 \Psi^{\text{Elast}}(\mathbf{C})}{\partial C_{IJ} \partial C_{KL}} = \frac{\lambda}{4} C_{IJ}^{-1} C_{KL}^{-1} + \frac{1}{4} [\mu - \lambda \log(J)] (C_{IK}^{-1} C_{JL}^{-1} + C_{IL}^{-1} C_{JK}^{-1}). \quad (\text{A.2c})$$

Flexoelectricity tensor μ .

The cubic flexoelectric tensor depends on the longitudinal μ_L , transversal μ_T and shear μ_S parameters (Le Quang and He, 2011, Codony et al., 2019). In the Cartesian axes, it takes the following form:

$$\mu_{LIJK} = \begin{cases} \mu_L, & \text{for } L = I = J = K, \\ \mu_T, & \text{for } I = J \neq K = L, \\ \mu_S, & \text{for } L = I \neq J = K \text{ or } L = J \neq I = K, \\ 0 & \text{otherwise.} \end{cases} \quad (\text{A.3})$$

Strain gradient elasticity tensor \mathbf{h} .

We consider an isotropic simplified strain gradient elasticity tensor (Altan and Aifantis, 1997), which depends on λ , μ and the length scale ℓ in the following form:

$$h_{IJKLMN} = (\lambda \delta_{IJ} \delta_{LM} + 2\mu \delta_{IL} \delta_{JM}) \ell^2 \delta_{KN}. \quad (\text{A.4})$$

Appendix B Second variation of the enthalpy functional

The second variation of the enthalpy functional, required in our solution method, is given by

$$\begin{aligned}
& \delta^2 \Pi[\chi, \phi; \delta\chi, \delta\phi; \Delta\chi, \Delta\phi] \\
&= \delta(R[\chi, \phi; \delta\chi, \delta\phi]) [\Delta\chi, \Delta\phi] \\
&= \frac{\partial R[\chi, \phi; \delta\chi, \delta\phi]}{\partial \chi} \Delta\chi + \frac{\partial R[\chi, \phi; \delta\chi, \delta\phi]}{\partial \phi} \Delta\phi \\
&= \int_{\Omega_0} \left\{ \delta \mathfrak{E}_{IJ} \Delta \mathfrak{E}_{KL} \left(4 \frac{\partial^2 \Psi^{\text{Elast}}(\mathbf{C})}{\partial C_{IJ} \partial C_{KL}} \right) + \left(2 \frac{\partial \Psi^{\text{Elast}}(\mathbf{C})}{\partial C_{IJ}} \right) (\Delta \delta) \mathfrak{E}_{IJ} \right. \\
&\quad + h_{IJKLMN} \delta \widetilde{\mathfrak{E}}_{IJK} \Delta \widetilde{\mathfrak{E}}_{LMN} + \left(h_{IJKLMN} \widetilde{\mathfrak{E}}_{LMN} \right) (\Delta \delta) \widetilde{\mathfrak{E}}_{IJK} \\
&\quad - \epsilon J C_{MF}^{-1} \delta E_F \Delta E_M \\
&\quad + \epsilon J \mathcal{C}_{MFIJ} E_F \left(\frac{1}{2} E_M (\Delta \delta) \mathfrak{E}_{IJ} + \delta \mathfrak{E}_{IJ} \Delta E_M + \delta E_M \Delta \mathfrak{E}_{IJ} \right) \\
&\quad + \epsilon J \widetilde{\mathcal{C}}_{MFIJKL} \frac{1}{2} E_M E_F \delta \mathfrak{E}_{IJ} \Delta \mathfrak{E}_{KL} \\
&\quad - \mu_{FABK} J C_{MF}^{-1} \left(E_M (\Delta \delta) \widetilde{\mathfrak{E}}_{ABK} + \delta E_M \Delta \widetilde{\mathfrak{E}}_{ABK} + \delta \widetilde{\mathfrak{E}}_{ABK} \Delta E_M \right) \\
&\quad + \mu_{FABK} J \mathcal{C}_{MFIJ} \left(\widetilde{\mathfrak{E}}_{ABK} (\delta \mathfrak{E}_{IJ} \Delta E_M + \delta E_M \Delta \mathfrak{E}_{IJ}) + E_M (\delta \mathfrak{E}_{IJ} \Delta \widetilde{\mathfrak{E}}_{ABK} + \delta \widetilde{\mathfrak{E}}_{ABK} \Delta \mathfrak{E}_{IJ}) + E_M \widetilde{\mathfrak{E}}_{ABK} (\Delta \delta) \mathfrak{E}_{IJ} \right) \\
&\quad \left. + \mu_{FABK} J \widetilde{\mathcal{C}}_{MFIJPQ} E_M \widetilde{\mathfrak{E}}_{ABK} \delta \mathfrak{E}_{IJ} \Delta \mathfrak{E}_{PQ} \right\} d\Omega_0 \\
&= \int_{\Omega_0} \left\{ \widetilde{S}_{IJ} (\Delta \delta) \mathfrak{E}_{IJ} + \widetilde{S}_{IJK} (\Delta \delta) \widetilde{\mathfrak{E}}_{IJK} \right. \\
&\quad + \left(\mathbb{A}_{IJKL}^{\text{Elast}} + \mathbb{A}_{IJKL}^{\text{Diele}} + \mathbb{A}_{IJKL}^{\text{Flexo}} \right) \delta \mathfrak{E}_{IJ} \Delta \mathfrak{E}_{KL} \\
&\quad + \widetilde{\mathbb{A}}_{IJKLMN}^{\text{SGEla}} \delta \widetilde{\mathfrak{E}}_{IJK} \Delta \widetilde{\mathfrak{E}}_{LMN} \\
&\quad + \widetilde{\mathbb{A}}_{IJKLM}^{\text{Flexo}} \left(\delta \mathfrak{E}_{IJ} \Delta \widetilde{\mathfrak{E}}_{KLM} + \delta \widetilde{\mathfrak{E}}_{KLM} \Delta \mathfrak{E}_{IJ} \right) \\
&\quad + \mathbb{B}_{IJ}^{\text{Diele}} (\delta E_I \Delta E_J) \\
&\quad + \left(\mathbb{C}_{IJK}^{\text{Diele}} + \mathbb{C}_{IJK}^{\text{Flexo}} \right) (\delta \mathfrak{E}_{IJ} \Delta E_K + \delta E_K \Delta \mathfrak{E}_{IJ}) \\
&\quad \left. + \widetilde{\mathbb{C}}_{IJKL}^{\text{Flexo}} \left(\delta E_L \Delta \widetilde{\mathfrak{E}}_{IJK} + \delta \widetilde{\mathfrak{E}}_{IJK} \Delta E_L \right) \right\} d\Omega_0,
\end{aligned} \tag{B.1}$$

where $\Delta\chi$ and $\Delta\phi$ are variations of χ and ϕ , respectively, and

$$\Delta E_L := -\frac{\partial(\Delta\phi)}{\partial X_L}, \quad (\text{B.2a})$$

$$\Delta F_{iI} := \frac{\partial(\Delta x_i)}{\partial X_I}, \quad (\text{B.2b})$$

$$\Delta \tilde{F}_{iIJ} := \frac{\partial^2(\Delta x_i)}{\partial X_I \partial X_J}, \quad (\text{B.2c})$$

$$\Delta \mathfrak{E}_{IJ} = \frac{\Delta C_{IJ}}{2} := \text{symm}_{IJ}(\Delta F_{kI} F_{kJ}), \quad (\text{B.2d})$$

$$\Delta \tilde{\mathfrak{E}}_{IJK} = \frac{\Delta \tilde{C}_{IJK}}{2} := \text{symm}_{IJ}(\Delta F_{kI} \tilde{F}_{kJK} + F_{kI} \Delta \tilde{F}_{kJK}), \quad (\text{B.2e})$$

$$(\Delta\delta)\mathfrak{E}_{IJ} = \frac{(\Delta\delta)C_{IJ}}{2} := \text{symm}_{IJ}(\Delta F_{kI} \delta F_{kJ}), \quad (\text{B.2f})$$

$$(\Delta\delta)\tilde{\mathfrak{E}}_{IJK} = \frac{(\Delta\delta)\tilde{C}_{IJK}}{2} := \text{symm}_{IJ}(\Delta F_{kI} \delta \tilde{F}_{kJK} + \delta F_{kI} \Delta \tilde{F}_{kJK}). \quad (\text{B.2g})$$

The material tensors in the right hand side of Eq. (B.1) are defined as follows:

$$\mathbb{A}_{IJKL}^{\text{Elast}}(\mathbf{C}) := \frac{\partial^2 \tilde{\Psi}^{\text{Elast}}}{\partial \mathfrak{E}_{IJ} \partial \mathfrak{E}_{KL}} \quad (\text{B.3a})$$

$$\mathbb{A}_{IJKL}^{\text{Diele}}(\mathbf{C}, \mathbf{E}) := \frac{\partial^2 \tilde{\Psi}^{\text{Diele}}}{\partial \mathfrak{E}_{IJ} \partial \mathfrak{E}_{KL}} = \frac{1}{2} J \tilde{\mathcal{C}}_{MFIJKL} E_M \epsilon E_F \quad (\text{B.3b})$$

$$\mathbb{A}_{IJKL}^{\text{Flexo}}(\mathbf{C}, \tilde{\mathbf{C}}, \mathbf{E}) := \frac{\partial^2 \tilde{\Psi}^{\text{Flexo}}}{\partial \mathfrak{E}_{IJ} \partial \mathfrak{E}_{KL}} = J \tilde{\mathcal{C}}_{MFIJKL} E_M \mu_{FABC} \tilde{\mathfrak{E}}_{ABC} \quad (\text{B.3c})$$

$$\tilde{\mathbb{A}}_{IJKLMN}^{\text{SGEla}} := \frac{\partial^2 \tilde{\Psi}^{\text{SGEla}}}{\partial \tilde{\mathfrak{E}}_{IJK} \partial \tilde{\mathfrak{E}}_{LMN}} = h_{IJKLMN}, \quad (\text{B.3d})$$

$$\tilde{\mathbb{A}}_{IJKLM}^{\text{Flexo}}(\mathbf{C}, \mathbf{E}) := \frac{\partial^2 \tilde{\Psi}^{\text{Flexo}}}{\partial \mathfrak{E}_{IJ} \partial \tilde{\mathfrak{E}}_{KLM}} = J \mathcal{C}_{ABIJ} \mu_{BKLM} E_A \quad (\text{B.3e})$$

$$\mathbb{B}_{IJ}^{\text{Diele}}(\mathbf{C}) := \frac{\partial^2 \tilde{\Psi}^{\text{Diele}}}{\partial E_I \partial E_J} = -\epsilon J C_{IJ}^{-1} \quad (\text{B.3f})$$

$$\mathbb{C}_{IJK}^{\text{Diele}}(\mathbf{C}, \mathbf{E}) := \frac{\partial^2 \tilde{\Psi}^{\text{Diele}}}{\partial \mathfrak{E}_{IJ} \partial E_K} = \epsilon J \mathcal{C}_{KMIJ} E_M \quad (\text{B.3g})$$

$$\mathbb{C}_{IJK}^{\text{Flexo}}(\mathbf{C}, \tilde{\mathbf{C}}) := \frac{\partial^2 \tilde{\Psi}^{\text{Flexo}}}{\partial \mathfrak{E}_{IJ} \partial E_K} = \mu_{MABC} J \mathcal{C}_{KMIJ} \tilde{\mathfrak{E}}_{ABC} \quad (\text{B.3h})$$

$$\tilde{\mathbb{C}}_{IJKL}^{\text{Flexo}}(\mathbf{C}) := \frac{\partial^2 \tilde{\Psi}^{\text{Flexo}}}{\partial \tilde{\mathfrak{E}}_{IJK} \partial E_L} = -\mu_{MIJK} J C_{ML}^{-1} \quad (\text{B.3i})$$

The tensor $\widetilde{\mathcal{C}}$ in Eq. (B.1) is defined as

$$\widetilde{\mathcal{C}}_{ABCDEF} := \frac{2}{J} \frac{\partial (J \mathcal{C}_{ABCD})}{\partial C_{EF}} = (\mathbb{D}_{ACBDEF} + \mathbb{D}_{BDACEF} + \mathbb{D}_{ADBCEF} + \mathbb{D}_{BCADEF} - \mathbb{D}_{ABCDEF} - \mathbb{D}_{CDABEF}), \quad (\text{B.4})$$

where $\mathbb{D}_{ABCDEF} := C_{AB}^{-1} \left(\frac{1}{2} C_{CD}^{-1} C_{EF}^{-1} - C_{CE}^{-1} C_{DF}^{-1} - C_{CF}^{-1} C_{DE}^{-1} \right)$.

Appendix C Analytical solutions for the displacement and the electric field in flexoelectric rods under bending

Following Bisshopp and Drucker (1945), Eq. (87) is integrated as

$$\frac{1}{2} \left(\frac{d\theta}{dS} \right)^2 + \beta^2 (\sin \theta^{\max} - \sin \theta) = 0, \quad (\text{C.1})$$

where $\theta(L) = \theta^{\max} \leq 0$ is the rotation at the free end of the rod produced by the applied load, and equivalently

$$dS = - \frac{d\theta}{\beta \sqrt{2(\sin \theta - \sin \theta^{\max})}}, \quad (\text{C.2})$$

since $\theta \leq 0$ and $d\theta/dS \leq 0$ for a rod bending downwards. The integral of Eq. (C.2) along the rod yields approximately its length, since

$$L = \int_0^L dS = \int_{\theta(0)}^{\theta(L)} \frac{dS}{d\theta} d\theta = \int_{\theta^{\max}}^0 \frac{d\theta}{\beta \sqrt{2(\sin \theta - \sin \theta^{\max})}}, \quad (\text{C.3})$$

and thus

$$\beta L = \int_{\theta^{\max}}^0 \frac{d\theta}{\sqrt{2(\sin \theta - \sin \theta^{\max})}}. \quad (\text{C.4})$$

In order to evaluate this integral, let us assume

$$\sin \theta^{\max} = 1 - 2p^2, \quad \sin \theta = 1 - 2p^2 \sin^2 \psi, \quad \psi \in [\psi_0, \frac{\pi}{2}], \quad (\text{C.5})$$

with

$$\psi_0 = \sin^{-1} \left(\frac{1}{p \sqrt{2}} \right) = \sin^{-1} \left(\frac{1}{\sqrt{1 - \sin \theta^{\max}}} \right). \quad (\text{C.6})$$

Using $\cos \theta = \sqrt{1 - \sin^2 \theta} = 2p \sin \psi \sqrt{1 - p^2 \sin^2 \psi}$, we obtain

$$d\theta = - \frac{2p \cos \psi}{\sqrt{1 - p^2 \sin^2 \psi}} d\psi, \quad (\text{C.7})$$

and substituting in Eq. (C.4) yields

$$\beta L = \int_{\psi_0}^{\pi/2} \frac{d\psi}{\sqrt{1 - p^2 \sin^2 \psi}}, \quad (\text{C.8})$$

which can be written as

$$\beta L = F(p) - F(p, \psi_0), \quad (\text{C.9})$$

where

$$F(p) = \int_0^{\pi/2} \frac{1}{\sqrt{1 - p^2 \sin^2 \psi}} d\psi, \quad \text{and} \quad F(p, \psi_0) = \int_0^{\psi_0} \frac{1}{\sqrt{1 - p^2 \sin^2 \psi}} d\psi. \quad (\text{C.10})$$

are the complete and incomplete elliptical integrals of the first kind, respectively (Jahnke, 1945). Hence, for a given value of θ^{\max} , β can be determined from Eq. (C.9) using Eqs. (C.5) and (C.6), and the corresponding applied vertical load producing the rotation θ^{\max} at the free end is then $N = \bar{Y} I^{\text{eff}} \beta^2$. For a given N , the problem is thus solved by the shooting method.

Using Eq. (60), the vertical displacement of the rod is

$$\begin{aligned} r_1(S) &= \int_0^S (1 + \zeta) \sin \theta d\tilde{S} \approx \int_0^\theta \frac{\sin \theta d\theta}{\beta \sqrt{2} (\sin \theta^{\max} - \sin \theta)} = \int_{\psi_0}^\psi \frac{2p^2 \sin^2 \tilde{\psi} - 1}{\beta \sqrt{1 - p^2 \sin^2 \tilde{\psi}}} d\tilde{\psi} \\ &= \frac{1}{\beta} [F(p, \psi) - F(p, \psi_0)] + \frac{2}{\beta} [\tilde{E}(p, \psi) - \tilde{E}(p, \psi_0)], \end{aligned} \quad (\text{C.11})$$

where

$$\tilde{E}(p) = \int_0^{\pi/2} \sqrt{1 - p^2 \sin^2 \psi} d\psi, \quad \text{and} \quad \tilde{E}(p, \psi_0) = \int_0^{\psi_0} \sqrt{1 - p^2 \sin^2 \psi} d\psi, \quad (\text{C.12})$$

are the complete and incomplete elliptical integrals of the second kind, respectively (Jahnke, 1945). Thus, the deflection of the rod at its loaded end is

$$r_1(L) = L + \frac{2}{\beta} [\tilde{E}(p, \psi_0) - \tilde{E}(p)]. \quad (\text{C.13})$$

Finally, the vertical electric field is computed from Eq. (73) as

$$E_1(S) = \frac{\mu_T}{\epsilon} \theta' = -\frac{\beta \mu_T}{\epsilon} \sqrt{2 (\sin \theta - \sin \theta^{\max})} = -\frac{\mu_T}{\epsilon} \sqrt{\frac{2N}{\bar{Y} I^{\text{eff}}}} (\sin \theta - \sin \theta^{\max}). \quad (\text{C.14})$$

Therefore, the electric field at the fixed end is

$$E_1(0) = -\frac{\mu_T}{\epsilon} \sqrt{\frac{2N}{\bar{Y} I^{\text{eff}}}} \sin |\theta^{\max}|. \quad (\text{C.15})$$

Appendix D Analytical solutions for displacement and electric field in flexoelectric rods under compressive axial load

Integration of Eq. (103) yields

$$\frac{1}{2} \left(\frac{d\theta}{dS} \right)^2 - \beta^2 (\cos \theta - \cos \theta^{\max}) = 0, \quad (\text{D.1})$$

where we assume upward buckling without loss of generality, and $\theta(L/4) = \theta^{\max} > 0$. Equivalently,

$$dS = \frac{d\theta}{\beta \sqrt{2(\cos \theta - \cos \theta^{\max})}}. \quad (\text{D.2})$$

Since the right end of the rod is allowed to move horizontally under the action of the compressive load, the length of the rod is assumed to remain approximately unaltered after buckling. Hence, using Eq. (D.2),

$$\frac{L}{4} = \int_{\theta(0)}^{\theta(L/4)} \frac{dS}{d\theta} d\theta = \int_0^{\theta^{\max}} \frac{d\theta}{\beta \sqrt{2(\cos \theta - \cos \theta^{\max})}}, \quad (\text{D.3})$$

and thus

$$\frac{\beta L}{4} = \int_0^{\theta^{\max}} \frac{1}{2 \sqrt{\sin^2 \frac{\theta^{\max}}{2} - \sin^2 \frac{\theta}{2}}} d\theta. \quad (\text{D.4})$$

To compute this integral, we define

$$\sin \frac{\theta^{\max}}{2} = p, \quad \sin \frac{\theta}{2} = p \sin \psi, \quad \psi \in [0, \frac{\pi}{2}]. \quad (\text{D.5})$$

Hence,

$$\beta L = 4F(p) = 4F\left(\sin \frac{\theta^{\max}}{2}\right), \quad (\text{D.6})$$

where again $F(p)$ is the complete elliptical integral of the first kind, see Eq. (C.10). So, for a given load N , θ^{\max} is determined by the shooting method, i.e. by giving values to θ^{\max} and computing the corresponding loading parameter β from Eq. (D.6) until the target $\beta = \sqrt{N/\bar{Y}I^{\text{eff}}}$ is reached.

Similarly, the change in the horizontal displacement, Δr_3 , can be evaluated by the difference of actual length (L) and the length projected over axial direction upon buckling as

$$\begin{aligned}\Delta r_3 &\approx L - 4 \int_{\theta(0)}^{\theta(\frac{L}{4})} \cos \theta \frac{dS}{d\theta} d\theta = L - \int_0^{\theta^{\max}} \frac{2 \cos \theta}{\beta \sqrt{\sin^2 \frac{\theta^{\max}}{2} - \sin^2 \frac{\theta}{2}}} d\theta = L - \frac{4}{\beta} \int_0^{\pi/2} \frac{1 - 2p^2 \sin^2 \psi}{\sqrt{1 - p^2 \sin^2 \psi}} d\psi \\ &= L - \frac{8\tilde{E}(p) - 4F(p)}{\beta} = \frac{8[F(p) - \tilde{E}(p)]}{\beta},\end{aligned}\quad (\text{D.7})$$

where we have used $\sqrt{\sin^2(\theta^{\max}/2) - \sin^2(\theta/2)} = p \cos \psi$, $\cos \theta / \cos(\theta/2) = \frac{1 - 2p^2 \sin^2 \psi}{\sqrt{1 - p^2 \sin^2 \psi}}$, and

Eq. (D.6), and again $\tilde{E}(p)$ is the complete elliptical integral of the second kind, see Eq. (C.12).

Since, the deformations in the half-rod are antisymmetric with respect to $S = L/4$, we split the vertical deflection into two parts. Hence, assuming that the rod buckles upwards without loss of generality,

$$\begin{aligned}S \in \left[0, \frac{L}{4}\right]: \quad r_1(S) &\approx \int_0^S \sin \theta(u) du = \int_0^\theta \frac{\sin \gamma d\gamma}{\beta \sqrt{2} (\cos \gamma - \cos \theta^{\max})} \\ &= \int_0^\psi \frac{2p \sin \xi d\xi}{\beta} = \frac{2p}{\beta} (1 - \cos \psi), \quad \psi \in [0, \frac{\pi}{2}]\end{aligned}\quad (\text{D.8a})$$

$$\begin{aligned}S \in \left[\frac{L}{4}, \frac{L}{2}\right]: \quad r_1(S) &\approx \frac{2p}{\beta} - \int_{\theta^{\max}}^\theta \frac{\sin \gamma d\gamma}{\beta \sqrt{2} (\cos \gamma - \cos \theta^{\max})} \\ &= \frac{2p}{\beta} + \int_{\frac{\pi}{2}}^\psi \frac{2p \sin(\frac{\pi}{2} - \xi) d\xi}{\beta} = \frac{2p}{\beta} \left(1 + \cos\left(\frac{\pi}{2} - \psi\right)\right), \quad \psi \in [0, \frac{\pi}{2}].\end{aligned}\quad (\text{D.8b})$$

(D.8c)

where we have used $\sqrt{\sin^2(\theta^{\max}/2) - \sin^2(\theta/2)} = p \cos \psi$, and $\sin \theta / \cos(\theta/2) = 2p \sin \psi$. Finally, the electric field can be evaluated as

$$\begin{aligned}S \in \left[0, \frac{L}{4}\right]: \quad E_1(S) &= \frac{\mu_T}{\epsilon} \theta' = \frac{\mu_T \beta}{\epsilon} \sqrt{2 (\cos \theta - \cos \theta^{\max})} = \\ &= \frac{\mu_T}{\epsilon} \sqrt{\frac{2N}{\bar{Y} I^{\text{eff}}}} (\cos \theta - \cos \theta^{\max}), \quad \theta \in [0, \theta^{\max}]\end{aligned}\quad (\text{D.9a})$$

$$S \in \left[\frac{L}{4}, \frac{L}{2}\right]: \quad E_1(S) = -\frac{\mu_T}{\epsilon} \sqrt{\frac{2N}{\bar{Y} I^{\text{eff}}}} \left(\cos\left(\theta\left(\frac{L}{2} - S\right)\right) - \cos \theta^{\max}\right), \quad \theta \in [0, \theta^{\max}] \quad (\text{D.9b})$$

Therefore, the vertical deflection and electric field at the center of the rod are

$$r_1\left(\frac{L}{2}\right) = \frac{4}{\beta} \sin\left(\frac{\theta^{\max}}{2}\right), \quad (\text{D.10})$$

$$E_1(0) = -E_1\left(\frac{L}{2}\right) = E_1(L) = \frac{\mu_T}{\epsilon} \sqrt{\frac{2N}{\tilde{Y}I^{\text{eff}}}} (1 - \cos \theta^{\max}). \quad (\text{D.11})$$

Appendix E Analytical solutions for displacement and voltage in flexoelectric rods under transversal voltage actuation

Similarly to [Appendix D](#), integration of the moment balance Eq. (135) yields

$$\frac{1}{2} \left(\frac{d\theta}{dS} \right)^2 - (1 + \zeta) \tilde{\beta}^2 (\cos \theta - \cos \theta^{\max}) = 0, \quad (\text{E.1})$$

where $\theta(L/4) = \theta^{\max}$ and upon integration

$$\frac{L}{4} = \int_0^{L/4} dS = \int_{\theta(0)}^{\theta(L/4)} \frac{dS}{d\theta} d\theta = \frac{1}{\sqrt{1 + \zeta}} \int_0^{\theta^{\max}} \frac{d\theta}{\tilde{\beta} \sqrt{2(\cos \theta - \cos \theta^{\max})}} = \frac{F(p)}{\tilde{\beta} \sqrt{1 + \zeta}}. \quad (\text{E.2})$$

Thus

$$\tilde{\beta} \sqrt{1 + \zeta} L = 4F(p) = 4F\left(\sin \frac{\theta^{\max}}{2}\right). \quad (\text{E.3})$$

In this case, the right end of the rod is clamped and thus the length of the rod after buckling is unknown, but its projection on the horizontal axis is the undeformed length L , therefore with the help of constraint Eq. (132)

$$\frac{L}{4} = \int_0^{L/4} dr_3 = \int_0^{\theta^{\max}} (1 + \zeta) \cos \theta \frac{dS}{d\theta} d\theta = \frac{\sqrt{1 + \zeta} [2\tilde{E}(p) - F(p)]}{\tilde{\beta}}. \quad (\text{E.4})$$

Therefore, by using Eqs. (E.3) and (E.4)

$$\zeta = \frac{F(p)}{2\tilde{E}(p) - F(p)} - 1. \quad (\text{E.5})$$

Once ζ is known, $\tilde{\beta}$ can be evaluated using Eq. (E.3) for any θ^{\max} .

Now, similar to [Appendix D](#),

$$\begin{aligned}
S \in \left[0, \frac{L}{4}\right]: \quad r_1(S) &= - \int_0^\theta \frac{(1 + \zeta) \sin \theta \, d\theta}{\tilde{\beta} \sqrt{1 + \zeta} \sqrt{2} (\cos \theta - \cos \theta^{\max})} \\
&= - \int_0^\psi \frac{2p \sqrt{1 + \zeta} \sin \psi \, d\psi}{\tilde{\beta}} = - \frac{2p \sqrt{1 + \zeta} (1 - \cos \psi)}{\tilde{\beta}}, \\
S \in \left[\frac{L}{4}, \frac{L}{2}\right]: \quad r_1(S) &= - \frac{\sqrt{1 + \zeta}}{\tilde{\beta}} \left(\int_0^{\theta^{\max}} \frac{\sin \theta \, d\theta}{\sqrt{2} (\cos \theta - \cos \theta^{\max})} - \int_{\theta^{\max}}^\theta \frac{\sin \theta \, d\theta}{\sqrt{2} (\cos \theta - \cos \theta^{\max})} \right) \\
&= - \frac{2p \sqrt{1 + \zeta} (1 + \cos \psi)}{\tilde{\beta}},
\end{aligned} \tag{E.6}$$

with $\sin \frac{\theta}{2} = p \sin \psi$. Hence, the deflection at the center of the rod and the curvature at the left end for downward buckling are

$$r_1\left(\frac{L}{2}\right) = - \frac{4p \sqrt{1 + \zeta}}{\tilde{\beta}}, \tag{E.7}$$

$$\theta'(0) = \tilde{\beta} \sqrt{2(1 + \zeta)(1 - \cos \theta^{\max})}. \tag{E.8}$$

References

- Amir Abdollahi and Irene Arias. Constructive and destructive interplay between piezoelectricity and flexoelectricity in flexural sensors and actuators. *Journal of Applied Mechanics*, 82(12), 2015. URL <https://doi.org/10.1115/1.4031333>.
- Amir Abdollahi, Christian Peco, Daniel Millán, Marino Arroyo, and Irene Arias. Computational evaluation of the flexoelectric effect in dielectric solids. *Journal of Applied Physics*, 116(9): 093502, 2014. URL <https://doi.org/10.1063/1.4893974>.
- Amir Abdollahi, Daniel Millán, Christian Peco, Marino Arroyo, and Irene Arias. Revisiting pyramid compression to quantify flexoelectricity: A three-dimensional simulation study. *Phys. Rev. B*, 91:104103, 2015a. URL <https://doi.org/10.1103/PhysRevB.91.104103>.
- Amir Abdollahi, Christian Peco, Daniel Millán, Marino Arroyo, Gustau Catalan, and Irene Arias. Fracture toughening and toughness asymmetry induced by flexoelectricity. *Phys. Rev. B*, 92: 094101, 2015b. URL <https://doi.org/10.1103/PhysRevB.92.094101>.
- BS Altan and EC Aifantis. On some aspects in the special theory of gradient elasticity. *Journal of the Mechanical Behavior of Materials*, 8(3):231–282, 1997. URL <https://doi.org/10.1515/JMBM.1997.8.3.231>.

- Li Anqing, Zhou Shenjie, Qi Lu, and Chen Xi. A flexoelectric theory with rotation gradient effects for elastic dielectrics. *Modelling and Simulation in Materials Science and Engineering*, 24(1): 015009, 2015. URL <https://doi.org/10.1088/0965-0393/24/1/015009>.
- S.S. Antman. *Nonlinear Problems of Elasticity*. Springer-Verlag, New York, 1995. ISBN 9780387276496. URL <https://doi.org/10.1007/0-387-27649-1>.
- S Baroudi and F Najar. Dynamic analysis of a nonlinear nanobeam with flexoelectric actuation. *Journal of Applied Physics*, 125(4):044503, 2019. URL <https://doi.org/10.1063/1.5057727>.
- Sivapalan Baskaran, Xiangtong He, Qin Chen, and John Y Fu. Experimental studies on the direct flexoelectric effect in α -phase polyvinylidene fluoride films. *Applied Physics Letters*, 98(24): 242901, 2011. URL <https://doi.org/10.1063/1.3599520>.
- Sivapalan Baskaran, Xiangtong He, Yu Wang, and John Y Fu. Strain gradient induced electric polarization in α -phase polyvinylidene fluoride films under bending conditions. *Journal of Applied Physics*, 111(1):014109, 2012. URL <https://doi.org/10.1063/1.3673817>.
- S Bauer and F Bauer. Piezoelectric polymers and their applications. In *Piezoelectricity*, pages 157–177. Springer, 2008. URL https://doi.org/10.1007/978-3-540-68683-5_6.
- KE Bisshopp and DC Drucker. Large deflection of cantilever beams. *Quarterly of Applied Mathematics*, 3(3):272–275, 1945. URL www.jstor.org/stable/43633516.
- Lance Breger, Takeo Furukawa, and Eiichi Fukada. Bending piezoelectricity in polyvinylidene fluoride. *Japanese Journal of Applied Physics*, 15(11):2239, 1976. URL <https://doi.org/10.1143/JJAP.15.2239>.
- É. V. Bursian and N. N. Trunov. Nonlocal piezoelectric effect. *Sov. Phys. Solid State*, 16(4):760 – 762, 1974. URL <https://www.tib.eu/de/suchen/id/tema-archive%3ATEMAE75020089214>.
- J M Bursian and O I Zaikovskii. Changes in curvature of a ferroelectric film due to polarization. *Soviet Physics Solid State*, 10(5):1121–1124, 1968.
- Baojin Chu and DR Salem. Flexoelectricity in several thermoplastic and thermosetting polymers. *Applied Physics Letters*, 101(10):103905, 2012. URL <https://doi.org/10.1063/1.4750064>.
- David Codony, Onofre Marco, Sonia Fernández-Méndez, and Irene Arias. An immersed boundary hierarchical b-spline method for flexoelectricity. *Computer Methods in Applied Mechanics and Engineering*, 354:750–782, 2019. URL <https://doi.org/10.1016/j.cma.2019.05.036>.

- C. de Boor. *A Practical Guide to Splines*. Applied Mathematical Sciences. Springer New York, 2001. ISBN 9780387953663. URL [10.1002/zamm.19800600129](https://doi.org/10.1002/zamm.19800600129).
- Feng Deng, Qian Deng, Wenshan Yu, and Shengping Shen. Mixed finite elements for flexoelectric solids. *Journal of Applied Mechanics*, 84(8), 2017. URL <https://doi.org/10.1115/1.4036939>.
- Feng Deng, Qian Deng, and Shengping Shen. A three-dimensional mixed finite element for flexoelectricity. *Journal of Applied Mechanics*, 85(3), 2018. URL <https://doi.org/10.1115/1.4038919>.
- Qian Deng, Mejdi Kammoun, Alper Erturk, and Pradeep Sharma. Nanoscale flexoelectric energy harvesting. *International Journal of Solids and Structures*, 51(18):3218–3225, 2014a. URL <https://doi.org/10.1016/j.ijsolstr.2014.05.018>.
- Qian Deng, Liping Liu, and Pradeep Sharma. Electrets in soft materials: Nonlinearity, size effects, and giant electromechanical coupling. *Physical Review E*, 90(1):012603, 2014b. URL <https://doi.org/10.1103/PhysRevE.90.012603>.
- Qian Deng, Liping Liu, and Pradeep Sharma. Flexoelectricity in soft materials and biological membranes. *Journal of the Mechanics and Physics of Solids*, 62:209–227, 2014c. URL <https://doi.org/10.1016/j.jmps.2013.09.021>.
- A Dorfmann and RW Ogden. Nonlinear electroelasticity. *Acta Mechanica*, 174(3-4):167–183, 2005. URL <https://doi.org/10.1007/s00707-004-0202-2>.
- Luis Dorfmann and Ray W Ogden. *Nonlinear theory of electroelastic and magnetoelastic interactions*, volume 1. Springer, 2014. URL <https://doi.org/10.1007/978-1-4614-9596-3>.
- Luis Dorfmann and Ray W Ogden. Nonlinear electroelasticity: material properties, continuum theory and applications. *Proceedings of the Royal Society A: Mathematical, Physical and Engineering Sciences*, 473(2204):20170311, 2017. URL <https://doi.org/10.1098/rspa.2017.0311>.
- John Y Fu, Wenyi Zhu, Nan Li, and L Eric Cross. Experimental studies of the converse flexoelectric effect induced by inhomogeneous electric field in a barium strontium titanate composition. *Journal of Applied Physics*, 100(2):024112, 2006. URL <https://doi.org/10.1063/1.2219990>.
- Hamid Ghasemi, Harold S Park, and Timon Rabczuk. A level-set based iga formulation for topology optimization of flexoelectric materials. *Computer Methods in Applied Mechanics and Engineering*, 313:239–258, 2017. URL <https://doi.org/10.1016/j.cma.2016.09.029>.

- Hamid Ghasemi, Harold S Park, and Timon Rabczuk. A multi-material level set-based topology optimization of flexoelectric composites. *Computer Methods in Applied Mechanics and Engineering*, 332:47–62, 2018. URL <https://doi.org/10.1016/j.cma.2017.12.005>.
- Prakhar Gupta and Ajeet Kumar. Effect of material nonlinearity on spatial buckling of nanorods and nanotubes. *Journal of Elasticity*, 126(2):155–171, 2017. URL <https://doi.org/10.1007/s10659-016-9586-1>.
- Ali R Hadjesfandiari. Size-dependent piezoelectricity. *International Journal of Solids and Structures*, 50(18):2781–2791, 2013. URL <https://doi.org/10.1016/j.ijsolstr.2013.04.020>.
- Khader M Hamdia, Hamid Ghasemi, Xiaoying Zhuang, Naif Alajlan, and Timon Rabczuk. Sensitivity and uncertainty analysis for flexoelectric nanostructures. *Computer Methods in Applied Mechanics and Engineering*, 337:95–109, 2018. URL <https://doi.org/10.1016/j.cma.2018.03.016>.
- John Harden, Badel Mbanga, Nandor Éber, Katalin Fodor-Csorba, Samuel Sprunt, James T Gleeson, and Antal Jakli. Giant flexoelectricity of bent-core nematic liquid crystals. *Physical review letters*, 97(15):157802, 2006. URL <https://doi.org/10.1103/PhysRevLett.97.157802>.
- Jiawang Hong and David Vanderbilt. First-principles theory of frozen-ion flexoelectricity. *Physical Review B*, 84(18):180101, 2011. URL <https://doi.org/10.1103/PhysRevB.84.180101>.
- ShuLing Hu and ShengPing Shen. Variational principles and governing equations in nano-dielectrics with the flexoelectric effect. *Science China Physics, Mechanics and Astronomy*, 53(8):1497–1504, 2010. URL <https://doi.org/10.1007/s11433-010-4039-5>.
- Shujin Huang, Lu Qi, Wenbin Huang, Longlong Shu, Shenjie Zhou, and Xiaoning Jiang. Flexoelectricity in dielectrics: Materials, structures and characterizations. *Journal of Advanced Dielectrics*, 8(02):1830002, 2018. URL <https://doi.org/10.1142/S2010135X18300025>.
- VL Indenbom, EB Loginov, and MA Osipov. Flexoelectric effect and structure of crystals. *Kristallografiya*, 28:1157–1162, 1981a.
- VL Indenbom, EB Loginov, and MA Osipov. Flexoelectric effect and crystal-structure. *Kristallografiya*, 26(6):1157–1162, 1981b.
- Eugene Jahnke. Tables of functions with formulae and curves. *New York: Dover Publications,—c1945, 4th ed.*, 1945. URL <https://ui.adsabs.harvard.edu/abs/1945tfwf.book.....J>.
- Xiaoning Jiang, Wenbin Huang, and Shujun Zhang. Flexoelectric nano-generator: Materials, structures and devices. *Nano Energy*, 2(6):1079–1092, 2013. URL <https://doi.org/10.1016/j.nanoen.2013.09.001>.

- Sh M Kogan. Piezoelectric effect during inhomogeneous deformation and acoustic scattering of carriers in crystals. *Soviet Physics-Solid State*, 5(10):2069–2070, 1964.
- Sana Krichen and Pradeep Sharma. Flexoelectricity: a perspective on an unusual electromechanical coupling. *Journal of Applied Mechanics*, 83(3), 2016. URL <https://doi.org/10.1115/1.4032378>.
- Lev Davidovich Landau and Evgenii Mikhailovich Lifshitz. *Course of theoretical physics*. Elsevier, 2013. URL <https://books.google.es/books?id=LuBbAwAAQBAJ>.
- M Lax and DF Nelson. Maxwell equations in material form. *Physical Review B*, 13(4):1777, 1976. URL <https://doi.org/10.1103/PhysRevB.13.1777>.
- H. Le Quang and Q.-C. He. The number and types of all possible rotational symmetries for flexoelectric tensors. *Proceedings of the Royal Society of London A: Mathematical, Physical and Engineering Sciences*, 467(2132):2369–2386, 2011. ISSN 1364-5021. URL <https://doi.org/10.1098/rspa.2010.0521>.
- Xu Liang, Shuling Hu, and Shengping Shen. Effects of surface and flexoelectricity on a piezoelectric nanobeam. *Smart materials and structures*, 23(3):035020, 2014. URL <https://doi.org/10.1088/0964-1726/23/3/035020>.
- EM Lifshitz and LD Landau. Statistical physics (course of theoretical physics, volume 5), 1984.
- Liwei Lin and Mu Chiao. Electro, thermal and elastic characterizations of suspended micro beams. *Microelectronics journal*, 29(4-5):269–276, 1998. URL [https://doi.org/10.1016/S0026-2692\(97\)00066-9](https://doi.org/10.1016/S0026-2692(97)00066-9).
- Liping Liu. An energy formulation of continuum magneto-electro-elasticity with applications. *Journal of the Mechanics and Physics of Solids*, 63:451–480, 2014. URL <https://doi.org/10.1016/j.jmps.2013.08.001>.
- Wenhui Ma and L Eric Cross. Large flexoelectric polarization in ceramic lead magnesium niobate. *Applied Physics Letters*, 79(26):4420–4422, 2001a. URL <https://doi.org/10.1063/1.1426690>.
- Wenhui Ma and L Eric Cross. Observation of the flexoelectric effect in relaxor Pb (Mg_{1/3} Nb_{2/3}) O₃ ceramics. *Applied Physics Letters*, 78(19):2920–2921, 2001b. URL <https://doi.org/10.1063/1.1356444>.
- Wenhui Ma and L Eric Cross. Flexoelectric polarization of barium strontium titanate in the paraelectric state. *Applied Physics Letters*, 81(18):3440–3442, 2002. URL <https://doi.org/10.1063/1.1518559>.

- Wenhui Ma and L Eric Cross. Strain-gradient-induced electric polarization in lead zirconate titanate ceramics. *Applied Physics Letters*, 82(19):3293–3295, 2003. URL <https://doi.org/10.1063/1.1570517>.
- Wenhui Ma and L Eric Cross. Flexoelectric effect in ceramic lead zirconate titanate. *Applied Physics Letters*, 86(7):072905, 2005. URL <https://doi.org/10.1063/1.1868078>.
- Wenhui Ma and L Eric Cross. Flexoelectricity of barium titanate. *Applied Physics Letters*, 88(23):232902, 2006. URL <https://doi.org/10.1063/1.2211309>.
- M. S. Majdoub, P. Sharma, and T. Çağın. Erratum: Enhanced size-dependent piezoelectricity and elasticity in nanostructures due to the flexoelectric effect [phys. rev. b 77, 125424 (2008)]. *Phys. Rev. B*, 79:119904, 2009. doi: 10.1103/PhysRevB.79.119904. URL <https://doi.org/10.1103/PhysRevB.79.119904>.
- MS Majdoub, P Sharma, and T Çağın. Enhanced size-dependent piezoelectricity and elasticity in nanostructures due to the flexoelectric effect. *Physical Review B*, 77(12):125424, 2008. URL <https://doi.org/10.1103/PhysRevB.77.125424>.
- Sheng Mao and Prashant K. Purohit. Insights into flexoelectric solids from strain-gradient elasticity. *ASME Journal of Applied Mechanics*, 81(8):1–10, 2014. URL <https://doi.org/10.1115/1.4027451>.
- Sheng Mao, Prashant K Purohit, and Nikolaos Aravas. Mixed finite-element formulations in piezoelectricity and flexoelectricity. *Proceedings of the Royal Society A: Mathematical, Physical and Engineering Sciences*, 472(2190):20150879, 2016. URL <https://doi.org/10.1098/rspa.2015.0879>.
- R Maranganti, ND Sharma, and P Sharma. Electromechanical coupling in nonpiezoelectric materials due to nanoscale nonlocal size effects: Green’s function solutions and embedded inclusions. *Physical Review B*, 74(1):014110, 2006. URL <https://doi.org/10.1103/PhysRevB.74.014110>.
- M Marvan and A Havránek. Flexoelectric effect in elastomers. In *Relationships of Polymeric Structure and Properties*, pages 33–36. Springer, 1998. URL <https://doi.org/10.1007/BFb0114342>.
- V.S. Mashkevich and K.B. Tolpygo. Electrical, optical and elastic properties of diamond type crystals. 1. *Soviet Physics JETP-USSR*, 5(3):435–439, 1957. URL <http://www.jetp.ac.ru/cgi-bin/e/index/e/5/3/p435?a=list>.
- Andrew McBride, Denis Davydov, and Paul Steinmann. Modelling the flexoelectric effect in solids: a micromorphic approach. *arXiv preprint*, 2019. URL <https://arxiv.org/abs/1909.08695>.

- Robert B Meyer. Piezoelectric effects in liquid crystals. *Physical Review Letters*, 22(18):918, 1969. URL <https://doi.org/10.1103/PhysRevLett.22.918>.
- Raymond David Mindlin. Micro-structure in linear elasticity. *Archive for Rational Mechanics and Analysis*, 16(1):51–78, 1964.
- Raymond David Mindlin. Polarization gradient in elastic dielectrics. *International Journal of Solids and Structures*, 4(6):637–642, 1968. URL [https://doi.org/10.1016/0020-7683\(68\)90079-6](https://doi.org/10.1016/0020-7683(68)90079-6).
- R.D. Mindlin and N.N. Eshel. On first strain-gradient theories in linear elasticity. *International Journal of Solids and Structures*, 4(1):109–124, 1968. URL [https://doi.org/10.1016/0020-7683\(68\)90036-X](https://doi.org/10.1016/0020-7683(68)90036-X).
- Anna N Morozovska, Eugene A Eliseev, Christian M Scherbakov, and Yulian M Vysochanskii. Influence of elastic strain gradient on the upper limit of flexocoupling strength, spatially modulated phases, and soft phonon dispersion in ferroics. *Physical Review B*, 94(17):174112, 2016. URL <https://doi.org/10.1103/PhysRevB.94.174112>.
- SS Nanthakumar, Xiaoying Zhuang, Harold S Park, and Timon Rabczuk. Topology optimization of flexoelectric structures. *Journal of the Mechanics and Physics of Solids*, 105:217–234, 2017. URL <https://doi.org/10.1016/j.jmps.2017.05.010>.
- BH Nguyen, X Zhuang, and Timon Rabczuk. Nurbs-based formulation for nonlinear electro-gradient elasticity in semiconductors. *Computer Methods in Applied Mechanics and Engineering*, 346:1074–1095, 2019. URL <https://doi.org/10.1016/j.cma.2018.08.026>.
- Thanh D. Nguyen, Sheng Mao, Yao-Wen Yeh, Prashant K. Purohit, and Michael C. McAlpine. Nanoscale flexoelectricity. *Advanced Materials*, 25(7):946–974, 2013. URL <https://doi.org/10.1002/adma.201203852>.
- Ailish O’Halloran, Fergal O’malley, and Peter McHugh. A review on dielectric elastomer actuators, technology, applications, and challenges. *Journal of Applied Physics*, 104(7):9, 2008. URL <https://doi.org/10.1063/1.2981642>.
- Ronald E Pelrine, Roy D Kornbluh, and Jose P Joseph. Electrostriction of polymer dielectrics with compliant electrodes as a means of actuation. *Sensors and Actuators A: Physical*, 64(1):77–85, 1998. URL [https://doi.org/10.1016/S0924-4247\(97\)01657-9](https://doi.org/10.1016/S0924-4247(97)01657-9).
- AG Petrov, RL Ramsey, and PNR Usherwood. Curvature-electric effects in artificial and natural membranes studied using patch-clamp techniques. *European Biophysics Journal*, 17(1):13–17, 1989. URL <https://doi.org/10.1007/BF00257141>.

- Alexander G Petrov. Flexoelectric model for active transport. In *Physical and Chemical Bases of Biological Information Transfer*, pages 111–125. Springer, 1975. URL https://doi.org/10.1007/978-1-4684-2181-1_9.
- Alexander G Petrov. Flexoelectricity of model and living membranes. *Biochimica et Biophysica Acta (BBA)-Biomembranes*, 1561(1):1–25, 2002. URL [https://doi.org/10.1016/S0304-4157\(01\)00007-7](https://doi.org/10.1016/S0304-4157(01)00007-7).
- L. Piegl and W. Tiller. *The NURBS Book*. Monographs in Visual Communication. Springer Berlin Heidelberg, 2012. ISBN 9783642973857. doi: 10.1007/978-3-642-97385-7. URL <https://books.google.es/books?id=58KqCAAQBAJ>.
- Roman Poya, Antonio J Gil, Rogelio Ortigosa, and Roberto Palma. On a family of numerical models for couple stress based flexoelectricity for continua and beams. *Journal of the Mechanics and Physics of Solids*, 125:613–652, 2019. URL <https://doi.org/10.1016/j.jmps.2019.01.013>.
- Jacques Prost and JP Marcerou. On the microscopic interpretation of flexoelectricity. *Journal de Physique*, 38(3):315–324, 1977. URL <https://doi.org/10.1051/jphys:01977003803031500>.
- Raffaele Resta. Towards a bulk theory of flexoelectricity. *Physical review letters*, 105(12):127601, 2010. URL <https://doi.org/10.1103/PhysRevLett.105.127601>.
- D.F. Rogers. *An Introduction to NURBS: With Historical Perspective*. Morgan Kaufmann Series in Computer Graphics and Geometric Modeling. Morgan Kaufmann Publishers, 2001. ISBN 9781558606692. URL <https://doi.org/10.1016/B978-1-55860-669-2.X5000-3>.
- Samuel Rosset and Herbert R Shea. Small, fast, and tough: Shrinking down integrated elastomer transducers. *Applied Physics Reviews*, 3(3):031105, 2016. URL <https://doi.org/10.1063/1.4963164>.
- E Sahin and S Dost. A strain-gradients theory of elastic dielectrics with spatial dispersion. *International Journal of Engineering Science*, 26(12):1231–1245, 1988. URL [https://doi.org/10.1016/0020-7225\(88\)90043-2](https://doi.org/10.1016/0020-7225(88)90043-2).
- Andrea Schiaffino, Cyrus E Dreyer, David Vanderbilt, and Massimiliano Stengel. Metric wave approach to flexoelectricity within density functional perturbation theory. *Physical Review B*, 99(8):085107, 2019. URL <https://doi.org/10.1103/PhysRevB.99.085107>.
- N.D. Sharma, C.M. Landis, and P. Sharma. Piezoelectric thin-film superlattices without using piezoelectric materials. *Journal of Applied Physics*, 108(2):1–25, 2010. doi: 10.1063/1.3443404. URL <http://dx.doi.org/10.1063/1.3443404>.

- Shengping Shen and Shuling Hu. A theory of flexoelectricity with surface effect for elastic dielectrics. *Journal of the Mechanics and Physics of Solids*, 58(5):665 – 677, 2010. ISSN 0022-5096. URL <https://doi.org/10.1016/j.jmps.2010.03.001>.
- Paul Steinmann and Duc Khoi Vu. Computational challenges in the simulation of nonlinear electroelasticity. *Computer Assisted Methods in Engineering and Science*, 19(3):199–212, 2017. URL <https://comes.ippt.pan.pl/index.php/comes/article/view/90>.
- Kai Sun. Toward molecular mechanoelectric sensors: Flexoelectric sensitivity of lipid bilayers to structure, location, and orientation of bound amphiphilic ions. *The Journal of Physical Chemistry B*, 101(33):6327–6330, 1997.
- A. K. Tagantsev. Piezoelectricity and flexoelectricity in crystalline dielectrics. *Phys. Rev. B*, 34: 5883–5889, 1986. URL <https://doi.org/10.1103/PhysRevB.34.5883>.
- AK Tagantsev. Theory of flexoelectric effect in crystals. *Zhurnal Eksperimental'noi i Teoreticheskoi Fiziki*, 88(6):2108–22, 1985. URL <http://www.jetp.ac.ru/cgi-bin/e/index/e/61/6/p1246?a=list>.
- Alexander K Tagantsev. Electric polarization in crystals and its response to thermal and elastic perturbations. *Phase Transitions: A Multinational Journal*, 35(3-4):119–203, 1991. URL <https://doi.org/10.1080/01411599108213201>.
- Tran Quoc Thai, Timon Rabczuk, and Xiaoying Zhuang. A large deformation isogeometric approach for flexoelectricity and soft materials. *Computer Methods in Applied Mechanics and Engineering*, 341:718–739, 2018. URL <https://doi.org/10.1016/j.cma.2018.05.019>.
- Stephen P Timoshenko and James M Gere. *Theory of elastic stability*. Courier Corporation, 2009. URL <https://books.google.es/books?id=98B6JOW2HiUC>.
- A Todorov, A Petrov, Michael O Brandt, and Janos H Fendler. Electrical and real-time stroboscopic interferometric measurements of bilayer lipid membrane flexoelectricity. *Langmuir*, 7 (12):3127–3137, 1991. URL <https://doi.org/10.1021/la00060a036>.
- AT Todorov, AG Petrov, and JH Fendler. First observation of the converse flexoelectric effect in bilayer lipid membranes. *The Journal of Physical Chemistry*, 98(12):3076–3079, 1994. URL <https://doi.org/10.1021/j100063a004>.
- KB Tolpygo. Long wavelength oscillations of diamond-type crystals including long range forces. *Soviet Physics-Solid State*, 4(7):1297–1305, 1963.
- CL Trabi, CV Brown, AAT Smith, and NJ Mottram. Interferometric method for determining the sum of the flexoelectric coefficients ($e_1 + e_3$) in an ionic nematic material. *Applied Physics Letters*, 92(22):223509, 2008. URL <https://doi.org/10.1063/1.2938722>.

- DK Vu, P Steinmann, and G Possart. Numerical modelling of non-linear electroelasticity. *International Journal for Numerical Methods in Engineering*, 70(6):685–704, 2007. URL <https://doi.org/10.1002/nme.1902>.
- Bo Wang, Yijia Gu, Shujun Zhang, and Long-Qing Chen. Flexoelectricity in solids: Progress, challenges, and perspectives. *Progress in Materials Science*, 2019. URL <https://doi.org/10.1016/j.pmatsci.2019.05.003>.
- P.V. Yudin and A.K. Tagantsev. Fundamentals of flexoelectricity in solids. *Nanotechnology*, 24(43):1–36, 2013. URL <https://doi.org/10.1088/0957-4484/24/43/432001>.
- PV Yudin, R Ahluwalia, and AK Tagantsev. Upper bounds for flexoelectric coefficients in ferroelectrics. *Applied Physics Letters*, 104(8):082913, 2014. URL <https://doi.org/10.1063/1.4865208>.
- PV Yudin, R Ahluwalia, and AK Tagantsev. Erratum: “upper bounds for flexoelectric coefficients in ferroelectrics” [appl. phys. lett. 104, 082913 (2014)]. *Applied Physics Letters*, 106(18):189902, 2015. URL <https://doi.org/10.1063/1.4919883>.
- Julien Yvonnet and LP Liu. A numerical framework for modeling flexoelectricity and Maxwell stress in soft dielectrics at finite strains. *Computer Methods in Applied Mechanics and Engineering*, 313:450–482, 2017. URL <https://doi.org/10.1016/j.cma.2016.09.007>.
- Runzhi Zhang, Xu Liang, and Shengping Shen. A timoshenko dielectric beam model with flexoelectric effect. *Meccanica*, 51(5):1181–1188, 2016a. URL <https://doi.org/10.1007/s11012-015-0290-1>.
- Shuwen Zhang, Minglong Xu, Xu Liang, and Shengping Shen. Shear flexoelectric coefficient μ_{1211} in polyvinylidene fluoride. *Journal of Applied Physics*, 117(20):204102, 2015. URL <https://doi.org/10.1063/1.4921444>.
- Shuwen Zhang, Minglong Xu, Guoliang Ma, Xu Liang, and Shengping Shen. Experimental method research on transverse flexoelectric response of poly (vinylidene fluoride). *Japanese Journal of Applied Physics*, 55(7):071601, 2016b. URL <https://doi.org/10.7567/JJAP.55.071601>.
- Yang Zhou, Jie Liu, Xinping Hu, Baojin Chu, Shutao Chen, and David Salem. Flexoelectric effect in PVDF-based polymers. *IEEE Transactions on Dielectrics and Electrical Insulation*, 24(2):727–731, 2017. URL <https://doi.org/10.1109/TDEI.2017.006273>.
- Xiaoying Zhuang, SS Nanthakumar, and Timon Rabczuk. A meshfree formulation for large deformation analysis of flexoelectric structures accounting for the surface effects. *arXiv preprint*, 2019. URL <https://arxiv.org/abs/1911.06553>.

- Xiaoying Zhuang, Binh Huy Nguyen, Subbiah Srivilliputtur Nanthakumar, Thai Quoc Tran, Naif Alajlan, and Timon Rabczuk. Computational modeling of flexoelectricity—a review. *Energies*, 13(6):1326, 2020. URL <https://doi.org/10.3390/en13061326>.
- P Zubko, G Catalan, A Buckley, PRL Welche, and JF Scott. Strain-gradient-induced polarization in SrTiO_3 single crystals. *Physical Review Letters*, 99(16):167601, 2007. URL <https://doi.org/10.1103/PhysRevLett.99.167601>.
- Pavlo Zubko, Gustau Catalan, and Alexander K. Tagantsev. Flexoelectric effect in solids. *Annual Review of Materials Research*, 24(43):387–421, 2013. URL <https://doi.org/10.1146/annurev-matsci-071312-121634>.